



# Observation and modeling of high-<sup>7</sup>Be events in Northern Europe associated with the instability of the Arctic polar vortex in early 2003

Erika Brattich<sup>1</sup>, Hongyu Liu<sup>2</sup>, Bo Zhang<sup>2</sup>, Miguel Ángel Hernández-Ceballos<sup>3</sup>, Jussi Paatero<sup>4</sup>, Darko Sarvan<sup>5</sup>, Vladimir Djurdjevic<sup>6</sup>, Laura Tositti<sup>7</sup>, and Jelena Ajtić<sup>5</sup>

- 5 <sup>1</sup> Department of Physics and Astronomy DIFA, Alma Mater Studiorum University of Bologna, via Irnerio 46, 40126 Bologna (BO), Italy  
<sup>2</sup> National Institute of Aerospace, 100 Exploration Way, Hampton, VA 23666, USA  
<sup>3</sup> Department of Physics, University of Cordoba, Rabanales Campus, 14071 Cordoba, Spain  
<sup>4</sup> Finnish Meteorological Institute, P.O. Box 503, FI-00101, Helsinki, Finland  
10 <sup>5</sup> Faculty of Veterinary Medicine, University of Belgrade, Bulevar oslobođenja 18, 11000 Belgrade, Serbia  
<sup>6</sup> Institute of Meteorology, Faculty of Physics, University of Belgrade, Studentski trg 18, 11000 Belgrade, Serbia  
<sup>7</sup> Department of Chemistry “G. Ciamician”, Alma Mater Studiorum University of Bologna, via Selmi 2, 40126 Bologna (BO), Italy

*Correspondence to:* Erika Brattich (erika.brattich@unibo.it)

- 15 **Abstract.** Events of very high concentrations of <sup>7</sup>Be cosmogenic radionuclide have been recorded in the subpolar regions of Europe during the cold season. With an aim to investigate the mechanisms responsible for those peak <sup>7</sup>Be events, and in particular to verify if they are associated with the fast descent of stratospheric air masses occurring during sudden stratospheric warming (SSWs), we analyse <sup>7</sup>Be observations at six sampling sites in Scandinavia during January-March 2003 when very high <sup>7</sup>Be concentrations were observed and the Arctic vortex  
20 was relatively unstable as a consequence of several SSWs. We use the GEOS-Chem chemistry and transport model driven by the MERRA-2 meteorological reanalysis to simulate tropospheric <sup>7</sup>Be over Northern Europe. We show that the model reasonably reproduces the temporal evolution of surface <sup>7</sup>Be concentrations observed at the six sampling sites. Our analysis of model simulations, surface <sup>7</sup>Be observations, as well as atmospheric soundings of ozone and temperature indicates that the <sup>7</sup>Be peak observed in late February 2003 (between 20 and 28 February  
25 2003) at the six sampling sites in Scandinavia was associated with downward transport of stratospheric vortex air originated during SSW that occurred a few days before the peak (18-21 February 2003).

## 1 Introduction

- Beryllium-7 (<sup>7</sup>Be) is a cosmogenic radionuclide widely monitored and analysed around the world (e.g.,  
30 Tositti et al., 2004, 2014; Gourdin et al., 2014; Sýkora et al., 2017). Due to its relatively long radiative half-life



(53.22 days) and its cosmogenic origin in the upper troposphere and lower stratosphere (UT-LS) (Lal and Peters, 1967),  $^7\text{Be}$  is considered a tracer of stratospheric influence and large-scale subsidence (e.g., Liu et al., 2016; Chae and Kim, 2019). The variability of the  $^7\text{Be}$  activity concentration in surface layers is driven by both static and dynamic factors, e.g., geographical location of the monitoring sites (e.g., Hernández-Ceballos et al., 2015), seasonal atmospheric processes driving transport of carrier aerosols (Lal and Peters, 1967), stratosphere-troposphere air mass exchange (Cristofanelli et al., 2003; Cristofanelli et al., 2009; Putero et al., 2016; Brattich et al., 2017a), synoptic and mesoscale patterns, vertical transport in the troposphere (Lee et al., 2007), solar activity and dry and wet deposition (e.g., Hernández-Ceballos et al., 2015, 2016a; Ioannidou and Papastefanou, 2006).

The spatial and temporal variability of the  $^7\text{Be}$  surface concentrations in Europe and their relationship with meteorological variables was previously analysed in many studies (e.g., Piñero García et al., 2012; Błażej and Mietelski, 2014). The impact of the 11-year solar modulation on the  $^7\text{Be}$  concentrations in the air is well established (e.g., Leppänen et al., 2010). The distinctive spring/summer maximum of  $^7\text{Be}$  concentrations is widely described and mainly linked with the increased downward transport from the upper troposphere resulting from the intense convection and higher tropopause height typical of the warm season (Cristofanelli et al., 2006; Gerasopoulos et al., 2001, 2003). In addition, cases of high  $^7\text{Be}$  surface concentration, some of which occurring over the autumn/winter season, have been analysed in Europe, e.g., over the Iberian Peninsula (Hernández-Ceballos et al., 2017) and at high-altitude stations in the Alps and the Apennines (Brattich et al., 2017; Cristofanelli et al., 2006, 2009). The spring/summer maximum was originally observed with fission products injected into the stratosphere during atmospheric nuclear tests (Dutkiewicz and Husain, 1985; Cristofanelli et al., 2018). A study of Salminen-Paatero et al. (2019) using potential vorticity analysis indicated that the transfer of stratospheric air into the troposphere was at its maximum in March followed by gradual movement into the ground-level air during spring and early summer.

Further, over the last decade many studies have investigated the  $^7\text{Be}$  records in Northern Europe (Leppänen et al., 2010, 2012; Leppänen and Paatero, 2013; Sarvan et al., 2017; Leppänen, 2019), one of the three regions in Europe identified with a distinct  $^7\text{Be}$  behaviour in the surface air (Ajtić et al., 2017; Hernández-Ceballos et al. 2015, 2016b). Among these studies, Ajtić et al. (2016) analysed the  $^7\text{Be}$  concentration measured in Helsinki, Finland, over 25 years (1987-2011), and pointed out a relatively high number of  $^7\text{Be}$  extremes occurring over autumn and winter: more specifically, 10 % of the highest  $^7\text{Be}$  concentrations (above 95<sup>th</sup> percentile) were observed in the cold season (October-March). Furthermore, recent studies have also indicated that the polar vortices can have a notable influence on the wintertime  $^7\text{Be}$  surface concentrations in both the Northern (Ajtić et al., 2018; Bianchi et al., 2019; Terzi and Kalinowski, 2017) and Southern Hemispheres (Pacini et al., 2015).



In particular, Ajtić et al. (2018) and Bianchi et al. (2019) employed two different methodologies to identify episodes of extremely high  $^7\text{Be}$  surface concentrations in the autumn and winter seasons, pointing out a large number of cases over the October-March period of the years investigated. The comparison of the dates identified in both analyses showed an overlap with the events of the so-called Sudden Stratospheric Warming (SSW) of the Arctic vortex, i.e., a sudden rise in the polar temperatures that leads to a highly irregular shape of the vortex and its misalignment from the pole. Ajtić et al. (2018) also noted cases of extremely high  $^7\text{Be}$  concentrations occurring right after a very low  $^7\text{Be}$  concentration over the Scandinavian Peninsula during autumn and winter. Overall, this relationship between the SSW of the Arctic vortex and high  $^7\text{Be}$  surface concentrations is likely linked to the perturbed stratosphere-troposphere interactions associated with SSWs, which could favor a fast descent of: 1) midlatitude air rich in  $^7\text{Be}$ , thus increasing this radionuclide's surface abundance, and 2) aged vortex air wherein  $^7\text{Be}$  is subjected to radioactive decay and not transported from outside the vortex, thus decreasing the  $^7\text{Be}$  surface abundance.

The atmospheric circulation in the Arctic is dominated by the presence of two distinct polar vortices, one in the troposphere and one in the stratosphere (Vaugh et al., 2017). The two vortices present well distinct features: first, the vortex in the troposphere is much more extended than the stratospheric one; and second, while the tropospheric vortex is present all-year round, the stratospheric polar vortex exists only from fall to spring (Vaugh et al., 2017). The stratospheric polar vortex in winter stems from the large-scale temperature gradients between the midlatitudes and the poles. Therefore, the stratospheric polar vortex begins to form in autumn as a result of the decreasing solar heating in the polar regions; it strengthens during winter and then breaks down in spring when solar radiation returns to the polar region. Larger topographic and land-sea contrasts and the resulting stronger upward-propagating waves in the Northern Hemisphere, make the northern stratospheric vortex, or the Arctic vortex, weaker and more distorted than its Southern Hemisphere counterpart, the Antarctic vortex. A higher temporal variability of the Arctic vortex includes the SSW. A major SSW can even cause the stratospheric vortex to break down during midwinter (Vaugh et al., 2017).

While the initial scientific interest over the stratospheric polar vortex was especially linked to the stratospheric ozone depletion and formation of the ozone holes over the poles, it is now recognized that the vortices might affect the processes in the troposphere and surface weather (e.g., Mitchell et al., 2013). The present work aims at investigating in detail the atmospheric processes responsible for high  $^7\text{Be}$  activities recorded in the cold season over the Scandinavian Peninsula and its relationship with the Arctic polar vortex through model simulations. For this purpose, we conduct  $^7\text{Be}$  simulations for the period of January-March 2003 using the GEOS-Chem global 3-D chemical and transport (CTM) model. The period was selected because of the large number of events with



extremely high  $^7\text{Be}$  concentrations at surface in Scandinavia; some of these events were preceded by very low surface concentrations in the lower troposphere ( $< 10^{\text{th}}$  percentile). This period thus offers the opportunity to test the hypothesis that SSWs ease a fast descent of not only the midlatitude but also vortex air (Ajtić et al., 2018.). To achieve this goal, our analysis will therefore focus on:

- Investigating the processes responsible for the variability of  $^7\text{Be}$  concentrations in surface air in Northern Europe;
- Better understanding whether and how SSW and the Arctic vortex winter-time instability influence the surface concentrations of  $^7\text{Be}$  in Northern Europe;
- Quantifying the rate of air subsidence on the inner and outer side of the vortex during the period of its instability.

To analyse the influence of SSW and of the Arctic polar vortex on  $^7\text{Be}$  concentrations, we first assess the performance of the GEOS-Chem model in reproducing the observed  $^7\text{Be}$  variability. We then use model simulations together with other supporting measurements from soundings and meteorological datasets to examine the processes responsible for the variability in the  $^7\text{Be}$  concentrations over the period of January-March 2003.

As opposite to the cosmogenic origin of  $^7\text{Be}$ ,  $^{210}\text{Pb}$  (half-life 22.3 years) is a nuclide of crustal origin derived from decay of  $^{222}\text{Rn}$  (half-life 3.8 days), which is emitted from soils by decay of  $^{226}\text{Ra}$ . Owing to the contrasting natural origins of the two nuclides, the  $^7\text{Be}/^{210}\text{Pb}$  ratio is often regarded as indicative of vertical transport processes and convective activity in the atmosphere (e.g., Koch et al., 1996; Tositti et al., 2004; Brattich et al., 2017a,b). After being produced by contrasting physical mechanisms, both  $^7\text{Be}$  and  $^{210}\text{Pb}$  rapidly attach to ambient submicron-sized particles (e.g., Gaffney et al., 2004) and are removed by wet (mainly) and dry (secondarily) deposition processes of their carrier aerosol. The bias in the simulated  $^7\text{Be}/^{210}\text{Pb}$  ratio due to uncertainties in the model deposition schemes is thus reduced. For this reason, besides  $^7\text{Be}$ , the  $^7\text{Be}/^{210}\text{Pb}$  ratio was also analysed to gain further insights into vertical transport processes during the study period.

The rest of this paper is organized as follows. Section 2 describes the radioactivity ( $^7\text{Be}$  and  $^{210}\text{Pb}$ ) and meteorological data used. Section 3 provides a brief description of GEOS-Chem, the HYSPLIT trajectory model, and statistical parameters used to assess the model's performance in reproducing the observations. Section 4 presents an overview of the  $^7\text{Be}$  observations made in Northern Europe in the boreal winter 2003. Section 5 analyses the precipitation and transport pattern in the study region, while Section 6 assesses how the GEOS-Chem model performs in reproducing the observed variability in the monthly mean surface  $^7\text{Be}$  concentrations during the study period. Section 7 further evaluates the performance of the model in reproducing the short-time variability of  $^7\text{Be}$  in



Northern Europe, followed by interpreting the observed variability using model simulations and additional meteorological observations in section 8. Finally, summary and conclusions are given in Section 9.

## 125 **2 Data**

In this section we briefly describe the  $^7\text{Be}$  and  $^{210}\text{Pb}$  radioactivity data as well as the meteorological datasets analysed in this work.

### **2.1 $^7\text{Be}$ data**

130 Since 1988, the Radioactivity Environmental Monitoring data bank (REMdb) (<https://rem.jrc.ec.europa.eu/RemWeb/>) has brought together and stored in a harmonised way environmental radioactivity data (air, water, milk and mixed diet) measured by the European Member States (Sangiorgi et al., 2019). Among the set of sample types and measurements recommended in 2000/473/Euratom (European Commission, 2000), measurements of natural radioelements, such as  $^7\text{Be}$  in surface air, are required, and hence, it is very closely monitored and widely stored in REMdb (De Cort et al., 2007).

135 Within the REMdb, the activity concentration of  $^7\text{Be}$  in the surface air in Northern Europe (latitude north of  $55^\circ\text{N}$ ) is available for six sampling sites (Hernández-Ceballos et al., 2015): Ivalo, Umea, Helsinki, Kista, Harku and Risoe, however, with varying start dates and sampling frequencies (Figure 1a). The largest dataset is for Helsinki where, since 1999, the sampling has been performed daily or once every two days. Datasets for Ivalo, Umea, Kista and Risoe also span more than two decades and have a good temporal coverage (roughly once a week  
140 since 1995).

### **2.2 $^{210}\text{Pb}$ data**

Daily aerosol samples were collected in Helsinki on the roof of the Finnish Meteorological Institute's main building ( $60^\circ 10'\text{N}$ ,  $24^\circ 57'\text{E}$ ). Filters (Munktell MGA, diameter  $\varnothing = 240$  mm) were changed every day at 06 UTC. The air volume was about  $3500$  m<sup>3</sup>/day. The filters were assayed for  $^{210}\text{Pb}$  by alpha counting of the in-grown  
145 daughter nuclide  $^{210}\text{Po}$  (Mattsson et al., 1996).

### **2.3 Meteorological data**

The  $^7\text{Be}$  variability is tightly linked to horizontal and vertical transport of the carrier aerosol, and to precipitation that leads to the radionuclide's removal from the atmosphere. Here we use the Modern-Era



Retrospective analysis for Research and Applications, Version 2 (MERRA-2) meteorological reanalysis (Gelaro et al., 2017) to assist in the data analysis and to drive the GEOS-Chem model simulations. MERRA-2 is produced with version 5.12.4 of the Goddard Earth Observing System (GEOS) atmospheric data assimilation system. It assimilates modern observations of the atmosphere, ocean, land, and chemistry, and includes assimilation of aerosol remote sensing data.

Vertical soundings of air temperature from the Finnish Meteorological Institute's (FMI) Arctic Space Centre (<http://fmiarc.fmi.fi>) at Sodankylä, northern Finland (67.37°N, 26.63°E) were obtained from the University of Wyoming (<http://weather.uwyo.edu/upperair/sounding.html>). Ozone sounding data (Kivi et al., 2007; Denton et al., 2019) was retrieved from the database of the FMI's Arctic Space Centre (<http://litdb.fmi.fi>). To study the effect of downward transport of stratospheric air masses into the troposphere, potential vorticity (PV) values (Holton et al., 1995) were calculated from wind, temperature, and surface pressure fields obtained from the European Centre for Medium-Range Weather Forecasts (ECMWF), Reading, UK.

### 3 Methods

In this section we give a brief description of the GEOS-Chem and HYSPLIT models and the statistical parameters used to indicate the model performances.

#### 3.1 GEOS-Chem model

GEOS-Chem (<http://www.geos-chem.org>) is a global 3-D CTM that has been widely used to study atmospheric composition and processes (e.g., Bey et al., 2001; Park et al., 2004; Eastham et al., 2014). In this study, we use the GEOS-Chem v11-01f to simulate  $^7\text{Be}$  and  $^{210}\text{Pb}$  and assist in interpreting the observations. GEOS-Chem includes a radionuclide simulation option ( $^{222}\text{Rn}$ - $^{210}\text{Pb}$ - $^7\text{Be}$ ), which simulates the emission, transport (advection, convection, boundary layer mixing), deposition and decay of the radionuclide tracers (Jacob et al., 1997; Liu et al., 2001; Yu et al., 2018).

We use the  $^7\text{Be}$  production rates recommended by Lal and Peters (1967) for a maximum solar activity year (1958), which has been shown to produce the best results compared to aircraft  $^7\text{Be}$  observations (Koch et al., 1996; Liu et al., 2001). The production rate is formulated as a function of latitude and pressure without seasonal variation (Koch et al., 1996). About two thirds of atmospheric  $^7\text{Be}$  is generated in the stratosphere.  $^{222}\text{Rn}$  emission follows a recent work by Zhang et al. (2020), in which a customized emission map was built upon a few previously published emission scenarios and evaluated against global  $^{222}\text{Rn}$  surface observations and aircraft profiles.  $^{222}\text{Rn}$  emission



flux rate is a function of latitude, longitude, and month.  $^7\text{Be}$  and  $^{210}\text{Pb}$  are assumed to behave like aerosols once formed in the atmosphere and subject to dry and wet deposition (Liu et al., 2001). Both wet and dry deposition for  $^{222}\text{Rn}$  are neglected due to its inert nature.

180 GEOS-Chem simulations in this work are driven by the MERRA-2 meteorological reanalysis. The native resolution of MERRA-2 is  $0.667^\circ$  longitude by  $0.5^\circ$  latitude, with 72 vertical layers (top at 0.01hPa). The meteorological fields are regridded into  $2.5^\circ$  longitude by  $2^\circ$  latitude for the GEOS-Chem simulations in this work. GEOS-Chem uses the TPCORE advection algorithm of Lin and Rood (1996). Convective transport is calculated using archived convective mass fluxes (Wu et al., 2007). Boundary-layer mixing is based on the non-local scheme  
185 implemented by Lin and McElroy (2010). The wet deposition scheme follows that of Liu et al. (2001) and includes rainout (in-cloud scavenging) due to stratiform and anvil precipitation, scavenging in convective updrafts (Mari et al., 2000), and washout (below-cloud scavenging) by precipitation (Wang et al., 2011). Precipitation formation and evaporation fields are archived in MERRA-2 and used directly by the model wet deposition scheme. Dry deposition is based on the resistance-in-series scheme of Wesely (1989).

190 In addition to the standard model simulations of  $^7\text{Be}$  and  $^{210}\text{Pb}$ , we also separately transport  $^7\text{Be}$  produced in the stratosphere to quantify the stratospheric contribution to  $^7\text{Be}$  in the troposphere. All model simulations are conducted for the period of January 2002 – March 2003 with initial conditions from previously archived restart files. Hourly and monthly mean outputs for January-March 2003 are used for analysis.

### 3.2 HYSPLIT

195 The Hybrid Single Particle Lagrangian Integrated Trajectory (HYSPLIT) model, developed by the NOAA's Air Resources Laboratory (ARL) (Stein et al., 2015), was used to calculate a set of backward trajectories during the study period. To compute the 96 h 3D backward trajectories at 00, 06, 12, and 18 UTC and with different ending heights: 100, 500, 1000 and 1500 m above ground level, the NCEP (National Centers for Environmental Prediction) FNL Operational Global Analysis (NCEP/NWS/NOAA/U.S. Department of Commerce, 2000) meteorological files  
200 were used. While 96 h was considered a sufficiently long period to represent the synoptic air flows, the heights were selected to help us to understand the behaviour of the airflows circulating in the Atmospheric Boundary Layer (ABL), just above the ABL, and in the free troposphere. We used the cluster methodology implemented in the HYSPLIT model to group the calculated trajectories according to their length and curvature, and thus identify the airflow patterns over the whole period of the analysis. It is worth mentioning that clusters, as well as trajectories,  
205 indicate an estimation of the general airflow rather than the exact pathway of an air parcel (e.g., Jorba et al., 2004; Salvador et al., 2008).





### 3.3 Evaluation of the model output

The performance of the model in reproducing observed activity concentrations is evaluated by calculating some basic statistical parameters, such as the mean and standard deviation and other indicators, according to the methodology developed by Hanna (1993) and summarized later by Chang and Hanna (2004). Specifically, the performance of the CTM was evaluated using the following set of indicators, proposed by Carruthers et al. (2004):

- The mean bias (*MB*), a measure of the mean difference between the modelled and observed concentrations:

$$MB = \overline{C_m - C_o} \quad (1)$$

where  $C_m$  is modelled concentration and  $C_o$  is observed concentration.

- The normalized mean square error (*NMSE*), a measure of the mean difference between matched pairs of modelled and observed concentrations:

$$NMSE = \frac{\overline{(C_m - C_o)^2}}{\overline{C_m C_o}} \quad (2)$$

- The fraction of modelled concentrations within a factor of 2 of observations (*FA2*), i.e., for which  $0.5 < C_m/C_o < 2$
- The Pearson's correlation coefficient (*R*), a measure of the extent of a linear relationship between the modelled and observed concentrations:

$$R = \frac{\sum_{i=1}^n (C_{o,i} - \overline{C_o})(C_{m,i} - \overline{C_m})}{\sqrt{\sum_{i=1}^n (C_{o,i} - \overline{C_o})^2 \sum_{i=1}^n (C_{m,i} - \overline{C_m})^2}} \quad (3)$$

A perfect model has *MB* and *NMSE* values equal to 0 and *FA2* value equal to 1, while the *R* results range from  $-1$  (perfect negative relationship) to  $+1$  (perfect positive relationship), where 0 implies no relationship between the variables. To better understand the quantitative differences between observations and simulations, scatter plots were used.

### 4 Boreal winter 2002/2003

As indicated by Ajtić et al. (2018) and Bianchi et al. (2019), the winter of 2003 offers a good opportunity to investigate a possible link between SSWs and extreme surface concentrations of  $^7\text{Be}$  detected in Northern Europe. This period is sufficiently covered by the  $^7\text{Be}$  activity concentration measurements at all six monitoring sites.





In particular, very high  $^7\text{Be}$  activity concentrations, above the 90<sup>th</sup> percentile simultaneously at most of the Scandinavian Peninsula sampling sites, were recorded around 23-24 February 2003 (Ajtić et al., 2016, 2018) (Figure 1b). During the 2002/2003 boreal winter, the Arctic vortex was relatively unstable, with six SSWs taking place over the whole season (Peters et al., 2010). Two very pronounced episodes, which were both associated with the vortex splitting and fast SSW recovery, occurred in January and February, respectively (Günther et al., 2008). The evolution of the vortex caused vortex filamentation and vigorous mixing of the vortex and midlatitude stratospheric air (Günther et al., 2008; Müller et al., 2003). Several balloon flights inside the Arctic polar vortex in early 2003 observed unusual trace gas distributions connected to an intrusion of mesospheric air down to altitudes of about 25 km (Engel et al., 2006; Huret et al., 2006; Müller et al., 2007). Since such disturbances around the pole are expected to affect the troposphere, i.e., on weather conditions (Baldwin and Dunkerton, 2001), and air composition (Hsu, 1980; Limpasuvan et al., 2004). Hence, the high  $^7\text{Be}$  concentrations that were measured in Scandinavia around 24 February 2003 could be a result of downward motion of midlatitude stratospheric air. Interestingly, prior to this episode, very low (below the 10<sup>th</sup> percentile for each site) surface concentrations of  $^7\text{Be}$  were measured in Risoe, Kista and Ivalo on 3, 10 and 16 February 2003, respectively (Figure 1). These low values were tentatively linked by Ajtić et al. (2018) with the transport of aged stratospheric vortex air poor in  $^7\text{Be}$ , even though they are more likely related to precipitation scavenging that occurred the days before, as shown by the ECA&D (European Climate Assessment & Dataset, <https://www.ecad.eu/>) records. The reader is referred to Ajtić et al. (2018) for more details.

## 5 Analysis of winter precipitation and transport in the Scandinavian Peninsula: observations vs. model simulations

Before analysing the temporal pattern of simulated  $^7\text{Be}$  concentrations, we analysed the precipitation and transport pattern in the MERRA-2 meteorological dataset that drives the GEOS-Chem simulations. In particular, the MERRA-2 precipitation was evaluated against the data from Global Precipitation Climatology Project (GPCP) satellite (<ftp://meso.gsfc.nasa.gov/pub/gpcp-v2.2/psg>) and surface observations in winter 2003.

Figure 2 shows the MERRA-2 and GPCP monthly precipitation in winter for the region within 0-90°N and 90°W – 90°E. Good agreement is found between the MERRA-2 and the GPCP precipitations averaged over the region. Specifically, the geographical distribution of precipitation in MERRA-2 shows some important features that are consistent with the observed climatology precipitations: the desert climate in North Africa with very low



precipitation throughout the period, high precipitation over the North Atlantic region during winter, and Europe where the seasonal pattern of precipitation is similar to that in the North Atlantic region.

To assess the capability of the model to correctly capture the trend in precipitation during the observation period at the sampling sites, we examined the normalized differences between the MERRA-2 and the observed precipitation, calculated as a difference between the MERRA-2 and the observed values, normalized over the observed value (Table 1).

Overall, the MERRA-2 precipitation tends to be generally higher than that of GPCP at all sampling sites (Table 1) except for Harku and Helsinki, and especially in the February-March period. This result is in agreement with the findings of Gelaro et al. (2017) who compared the global precipitation of MERRA-2 and GPCP, and reported a general positive bias over northern high latitudes. However, the agreement between MERRA-2 and GPCP precipitation seasonality is reasonable, as indicated by the correlation coefficient values, higher than 0.85 at all sites except for Ivalo (-0.32), and the low NMSE values, in the range of 0-0.42 (Table 1).

Figure 3 shows that winter circulation in the Scandinavian Peninsula is dominated by SW and W winds (Chen, 2000; Linderson, 2001). The analysis of the main circulation in the three months in Figure 3 reveals low wind speeds from S-SW in the study area and period. A region of strong wind speeds, possibly corresponding to the Arctic vortex, is clearly visible at surface level to the west of the study area in all the three months. In addition, there appears to be a convergence area (opposite wind directions) between 60 and 75°N. Model-simulated  $^7\text{Be}/^{210}\text{Pb}$  ratios and fraction of stratospheric  $^7\text{Be}$  increase over the three months period and peak in March, suggesting increasing stratospheric influence, subsidence, or convective mixing in the study region.

## 280 **6 Variations of the monthly mean surface $^7\text{Be}$ concentrations in the Arctic region: model simulations vs. observations**

Figure 4a shows a scatter plot comparing the simulated and observed monthly mean  $^7\text{Be}$  concentrations at the six sampling sites. Table 2 reports the statistical parameters and the normalized differences that indicate the performance of the GEOS-Chem model in reproducing the observed  $^7\text{Be}$  monthly means.

In general, the model well simulates the month-to-month trend in  $^7\text{Be}$  concentrations measured at the sampling sites, as indicated by the fact that all the values fall within the 95% confidence levels (Figure 4a) and the high positive correlation coefficients ( $> 0.7$ ) except for Ivalo and the low MB and NMSE values (Table 2). In fact, the normalized differences are not very high (generally  $< 1$ ), except at Risoe. The bias between the model and the observations is partly attributed to the coarse resolution of the model. Overall, the simulations underestimate the



290 observed values, likely due to uncertainties associated with the deposition schemes and/or precipitation as discussed earlier.

The use of the  $^7\text{Be}$  production rate of Lal and Peters (1967) for a solar maximum year (1958) may also partly explain the tendency of simulated  $^7\text{Be}$  to be lower than observed. The sunspot number in 2003 (99.3) was rather low (slowly decreasing from 2000, a solar maximum year, and reaching minimum in 2008) if compared to  
295 the 1958 value of 184.8. As known, the galactic cosmic-ray intensity, largely responsible for the production of cosmogenic radionuclides, at the Earth's orbit is inversely related to solar activity (O'Brien, 1979), leading to the well-known phase opposition between sunspot number and  $^7\text{Be}$  concentration (e.g., Hernández-Ceballos et al., 2015). Sunspot number data herein used were extracted from the World Data Center for the production, preservation and dissemination of the international sunspot number (Sunspot Index and Long-term Solar  
300 Observation, SILSO, Royal Observatory of Belgium, Brussels, <http://www.sidc.be/silso/datafiles> - total).

### **7 Variations of the $^7\text{Be}$ weekly and daily mean surface concentrations in the Arctic region: observations vs. model simulations**

After analysing the model's performance in reproducing  $^7\text{Be}$  monthly mean observations in the previous Section, we compare here in Figure 4b simulated and observed weekly (daily in the case of Helsinki)  $^7\text{Be}$  activity  
305 concentrations at the six sampling sites. Table 3 shows the corresponding parameters that indicate the performance of the GEOS-Chem model in reproducing observations. The weekly evolution of simulated versus observed  $^7\text{Be}$  concentrations at these sites is shown in Figure 5.

As with the monthly means, the model generally represents adequately the temporal pattern but not the magnitude of weekly mean concentrations, which tend to be lower than those observed (Table 3, Figures 4b and  
310 5). This can arise from the higher precipitation in the model than in the observations and/or from errors in the deposition schemes. However, the correct reproduction of the  $^7\text{Be}$  temporal pattern, as indicated by the high correlation values at all sampling sites with the exception of Risoe, suggests that the model captures the transport processes leading to the peak in  $^7\text{Be}$  concentrations at the end of February 2003 and the preceding very low concentration values. In addition, the low MB and NMSE values calculated at all sites and especially at Ivalo and  
315 Umea suggest that the model reproduces adequately the observed values (Figure 5).

As for the  $^7\text{Be}/^{210}\text{Pb}$  ratio in Helsinki (Table 3), the model tends to underestimate the observed ratio, which could be due to the model underestimating  $^7\text{Be}$  and overestimating  $^{210}\text{Pb}$ . Nevertheless, the relatively high



correlation between the simulated and observed ratios suggests a reasonable simulation of the temporal pattern of this tracer.

## 320 **8 Understanding the $^7\text{Be}$ variations during the 2002/2003 boreal winter**

As mentioned earlier (Section 4), an SSW event occurred at the end of February 2003. We concentrated our analysis on two different periods during the month: early in the month, between 3 and 16 February when very low  $^7\text{Be}$  concentration values were recorded, and at the end of the month between 20 and 28 February characterized by extremely high  $^7\text{Be}$  concentrations. To gain further insights into the  $^7\text{Be}$  variations during the 2002/2003 boreal  
325 winter (Section 7), we analysed the simulated  $^7\text{Be}/^{210}\text{Pb}$  ratio, maps of surface winds and relative humidity, ozone soundings, vertical cross sections of simulated  $^7\text{Be}$  activity concentrations and calculated potential vorticity, and simulated and observed vertical profiles of air temperature. The results were further supported with the analysis of the clusters of back-trajectories during the two different periods of low and high  $^7\text{Be}$  concentrations.

During the 2002/2003 boreal winter, the Arctic vortex was relatively unstable, with six SSWs taking place  
330 over the whole season (Peters et al., 2010), and two very pronounced SSWs, with the vortex splitting and re-establishing within a few days, occurred in January and February (Günther et al., 2008). On one hand, this evolution of the vortex caused vortex filamentation and vigorous mixing of the vortex and midlatitude stratospheric air (Günther et al., 2008; Müller et al., 2003). On the other hand, such disturbances around the pole were also expected to propagate through the troposphere, i.e., on weather conditions (Baldwin and Dunkerton, 2001), and air  
335 composition (Hsu, 1980; Limpasuvan et al., 2004). Hence, the high  $^7\text{Be}$  concentrations measured in Scandinavia around 24 February 2003 could be the result of downward transport of midlatitude stratospheric air. Interestingly, prior to this episode, very low (below the 10<sup>th</sup> percentile for each site) surface concentrations of  $^7\text{Be}$  were measured in Risoe, Kista and Ivalo on 3, 10 and 16 February 2003, respectively (Figure 1b), as connected to precipitation scavenging that occurred the days before, as discussed earlier.

Figure 6 presents the temporal (weekly mean) pattern of  $^7\text{Be}/^{210}\text{Pb}$  and of the stratospheric fraction of  $^7\text{Be}$   
340 (calculated as the ratio of the stratospheric  $^7\text{Be}$  tracer concentration to the total  $^7\text{Be}$  concentration in the troposphere) at the six sampling sites, while daily observations of the  $^7\text{Be}/^{210}\text{Pb}$  ratio at Helsinki and Sodankylä (67.367°N, 26.629°E; 160 km south of Ivalo) are presented in the Supplementary Information (hereafter SI). At the beginning of February, the ratio was generally quite low at all the sites. In contrast, the week of 19-26 February 2003 was  
345 marked by an evident peak in the  $^7\text{Be}/^{210}\text{Pb}$  ratio and a simultaneous increase in the fraction of  $^7\text{Be}$  originating in



the stratosphere at all sites, which together could be the first indication of a prominent vertical transport from the UT-LS region.

Hence, we further examined the vertical profiles of temperature with an aim to identify differences in vertical transport near the beginning and end of February. The soundings from the Sodankylä station in the Arctic offer three sets of measurements for each of the investigated periods: on 10 and 16 February, that fall into the period when very low  $^7\text{Be}$  concentrations were recorded in Kista and Ivalo, respectively; and 22 and 24 February, the days marked by extremely high  $^7\text{Be}$  concentrations over the Scandinavian Peninsula; 20 and 21 February in the period of transition to high  $^7\text{Be}$  concentration over the Scandinavian Peninsula. Figure 7 shows air temperature profiles in the MERRA-2 dataset and atmospheric soundings at the Sodankylä station. Besides the very good agreement between the simulated and observed temperatures, a warming of the stratosphere (20-60 km) and a different vertical temperature structure of the lower stratosphere around 20-24 February as compared to the 10 and 16 February profiles are also evident. This observation is a clear indication of the link between the SSW and the  $^7\text{Be}$  peak observed at the six sampling sites located in Northern Europe. In addition, the ozone soundings at the Sodankylä station reveal an ozone mixing ratio peak in the lower troposphere ( $\sim 1.5\text{-}3\text{km}$ ) on 19<sup>th</sup> February 2003 as compared to those observed during 12, 26 and 28 February 2003 (Figure 8), consistent with downward transport from higher altitudes around that day. Despite the chemical ozone loss in the Arctic vortex in the stratosphere in 2003 as observed by ozone soundings (Tilmes et al., 2006), obviously lower-stratospheric ozone was still enhanced relative to tropospheric ozone.

Simultaneously, the analysis of maps of surface transport and relative humidity (Figure 9) highlights the different winds and relative humidity values in the two periods, with low relative humidity values ( $\sim 40\text{-}50\%$ ) suggesting subsidence from 18 to 21 February, and the transition from a clockwise circulation to the fast and complex wind system typical of the second period corresponding to the high  $^7\text{Be}$  peak and the SSW. Interestingly, the parcel of the lowest relative humidity values occurs during the 18-21 February period, i.e., a couple of days before the dates of the  $^7\text{Be}$  peaks in the measurements and those peaks in the simulated  $^7\text{Be}/^{210}\text{Pb}$  ratio and stratospheric  $^7\text{Be}$  fraction (Figure 1b and Figure 6). Together with enhanced ozone concentrations observed in the lower troposphere on 19<sup>th</sup> February, this suggests that the downward transport from the UT-LS was triggered by the SSW occurring a few days before.

To better constrain the stratospheric origin of the air masses arriving at the sampling sites during the two periods, we further analyzed the potential vorticity data from ECMWF during the month of February 2003 at three latitudes (63, 64.5 and 66°N) along the 21°E meridian (Figure 10). The data reveal clearly a bubble of high potential vorticity down to the surface at the three latitudes from 18 till 22 February 2003, particularly at the northernmost



latitude where values are higher than 1.6 PVU, a value considered as a threshold for stratospheric air in the lower troposphere especially when in conjunction with low relative humidity, high  $^7\text{Be}/^{210}\text{Pb}$  ratios and ozone (Cristofanelli et al., 2006) were observed.

380 The low relative humidity (Figure 9) and high potential vorticity (Figure 10) corresponded to high  $^7\text{Be}$  descending to lower atmospheric levels, as simulated by the model (Figure 11). The descending vertical motion from the upper vertical levels during the period is clearly visible in the MERRA-2 pressure vertical velocity (omega) fields sampled at the six sampling sites for the month of February 2003, especially for the northernmost sites (Figure 12). Further evidence of this is seen from the maps of pressure vertical velocity (Figure 13) and of the  
385 stratospheric fraction of  $^7\text{Be}$  originated in the stratosphere (Figure 14) at 940 hPa in the boundary layer.

Analysis and comparison of 4-day back-trajectories at each sampling station allowed a reconstruction of two distinct atmospheric circulation patterns in the two periods. Figure 15 shows the clustering results for three sampling sites (Ivalo, Harku, Risoe) during both periods. The stations are ordered as a function of decreasing latitude from high (upper panels) to low (lower panels). Only results at 1000 m are shown and cluster results for  
390 other altitudes in the lower troposphere are similar. While the first period (with low  $^7\text{Be}$  values) presents the dominance of westerly winds (air masses flowing eastward), as typical of these latitudes (Zanis et al., 1999), the second period is characterized by a clockwise displacement of airflows with origins at higher altitudes (Figure 15). This pattern in the second period is better established at lower latitude stations (Helsinki, Harku, Kista and Risoe) compared to higher latitude ones (Ivalo, Umea). It likely results from the aged vortex (Günther et al., 2008) and  
395 the SSW at the end of February, corresponding to a decrease in the MERRA-2 daily average height of the thermal tropopause on 21<sup>st</sup>-22<sup>nd</sup> February at the Sodankylä station in Finland (Figure S3) during the SSW (Peethani et al., 2014; Wargan and Coy, 2016). Associated with these processes is the downward transport of stratospheric air previously identified with an independent approach.

## 9 Summary and conclusions

400 We have used a global 3-D model (GEOS-Chem) driven by the MERRA-2 meteorological reanalysis to simulate atmospheric concentrations of  $^7\text{Be}$  of cosmogenic origin for the period of January-March 2003. The aim was to verify the mechanisms responsible for the surface  $^7\text{Be}$  variabilities in Northern Europe, and to test the hypothesis that SSWs may facilitate fast descent of UT-LS vortex air to the surface. The period was selected as it involves two intense SSWs and observations of extremely high  $^7\text{Be}$  concentrations at six sampling sites in  
405 Scandinavia.





Before using the model's output to investigate the processes responsible for  $^7\text{Be}$  variability in Northern Europe over the period, we evaluated the MERRA-2 precipitation fields against the GPCP satellite and surface observations. A generally good agreement was found both at regional scale and at the six sampling sites. Analysis of the wind fields in the study period indicates low wind speeds from S-SW in agreement with the major circulation patterns over the Scandinavian Peninsula in winter, and the presence of a region of strong wind speeds to the west of the study area, likely in connection with the Arctic polar vortex.

The model reproduces efficiently the  $^7\text{Be}$  and  $^7\text{Be}/^{210}\text{Pb}$  temporal (i.e., monthly and weekly) patterns at the six sampling sites in the study period, even though it tends to underestimate the observed surface  $^7\text{Be}$  concentrations. The lower modelled values are likely due to its coarse resolution ( $2.5^\circ$  longitude by  $2^\circ$  latitude), lack of year-to-year variation in  $^7\text{Be}$  production rates, and uncertainties associated with precipitation scavenging.

In order to investigate the processes responsible for  $^7\text{Be}$  variability at the six sampling sites during the study period, and in particular to test whether the peak  $^7\text{Be}$  concentrations measured in Scandinavia around 24 February 2003 originated from fast descent of stratospheric vortex air facilitated by SSW, we analysed time-height cross sections of simulated  $^7\text{Be}$  and potential vorticity, vertical profiles of air temperature, maps of surface winds and relative humidity, and ozone soundings. The analysis of the temporal variations of simulated  $^7\text{Be}/^{210}\text{Pb}$  ratio and fraction of  $^7\text{Be}$  originated in the stratosphere indicates a peak during the week of 19-26 February 2003, suggesting downward transport from the UT-LS region. The latter is corroborated by a layer of ozone mixing ratio enhancements in the lower troposphere recorded by the soundings at the Sodankylä station on 19<sup>th</sup> February. Furthermore, the vertical profiles of air temperature indicate a warming of the stratosphere and a change in shape in to the vicinity of the tropopause region during the period, suggesting the link between the downward transport of the vortex air and SSW.

Our analysis of time-height cross sections of simulated  $^7\text{Be}$  concentrations, calculated potential vorticity and MERRA-2 pressure vertical velocity ( $\omega$ ) reveals the vertical downward transport to the surface a stratospheric air parcel characterized by high potential vorticity, high vertical velocity (in particular at Ivalo on 19<sup>th</sup> February) and high  $^7\text{Be}$  concentrations, further supporting the stratospheric origin of the air masses during the investigated period.

Additionally, low relative humidity and a change in the circulation pattern from slow, clockwise to fast, swirling winds occurred over the study area. The change in the circulation pattern and the downward transport of stratospheric air was verified by the analysis of the clusters of back trajectories during the periods of low and high  $^7\text{Be}$  concentrations, which showed a change from westerlies to airflows from upper vertical levels.





Altogether, these analyses confirm the link between the SSW and transport of stratospheric air to the surface, resulting in high surface  $^7\text{Be}$  concentrations observed in February 2003 in Scandinavia. Since more frequent SSWs are expected in a warmer climate (Kang and Tziperman, 2017), this link has important implications for the impact of climate change on atmospheric transport, tropospheric composition, and air quality in northern high-latitude regions.

### Data availability

The  $^7\text{Be}$  and  $^{210}\text{Pb}$  observational data are described in Section 2.1 and 2.2, respectively. The  $^{222}\text{Rn}$  and  $^7\text{Be}$  emission data used in this paper is described in Section 3.1.  $^7\text{Be}$  activity concentration data are available in the Radioactivity Environmental Monitoring (REM) database (<https://data.jrc.ec.europa.eu/collection/id-0117>). All model output, and  $^{210}\text{Pb}$  daily observational data at Helsinki and Sodankylä for January-March 2003 are available online (<http://doi.org/10.5281/zenodo.4117521>).

### Author contributions

JA, MAHC and EB designed the study. HL and BZ conducted the GEOS-Chem model simulations. MAHC led the calculation and analysis of HYSPLIT back-trajectories. EB developed the analysis methodology and led the analysis of observational data and model output, with contributions from all coauthors. JP contributed  $^{210}\text{Pb}$  and meteorological observational datasets. EB wrote the manuscript with contributions from all coauthors.

### Competing interests

The authors declare that they have no conflict of interest.

### Acknowledgements

The paper is part of the research conducted within the project "Climate changes and their influence on the environment: impacts, adaptation and mitigation" (No. 43007) financed by the Ministry of Education, Science and Technological Development of the Republic of Serbia (2011–2019). HL and BZ acknowledge funding support from the NASA Modeling, Analysis and Prediction Program (grant 80NSSC17K0221) and Atmospheric Composition Campaign Data Analysis and Modeling program (grant NNX14AR07G). NASA Center for



460 Computational Sciences (NCCS) provided supercomputing resources. The GEOS-Chem model is managed by the  
Atmospheric Chemistry Modeling Group at Harvard University with support from NASA ACPMAP and MAP  
programs. The University of Wyoming, Dr. Rigel Kivi from the Finnish Meteorological Institute Arctic Space  
Center and Dr. Laura Thölix from the Finnish Meteorological Institute are gratefully acknowledged for providing  
and helping with temperature profiles, ozone soundings and potential vorticity data used to support the detection  
465 of air masses of stratospheric origin in the troposphere. The World Data Center is gratefully acknowledged for the  
production, preservation and dissemination of the international sunspot number (Sunspot Index and Long-term  
Solar Observation, SILSO, Royal Observatory of Belgium, Brussels, <http://www.sidc.be/silso/datafiles#total>). The  
NOAA/ESRL Physical Sciences Laboratory Boulder Colorado is gratefully acknowledged for providing data and  
plots from the Twentieth Century Reanalysis Project version 3 through their web site (<http://psl.noaa.gov>). Support  
470 for the Twentieth Century Reanalysis Project version 3 dataset is provided by the U.S. Department of Energy,  
Office of Science Biological and Environmental Research (BER; <http://science.energy.gov/ber/>), by the National  
Oceanic and Atmospheric Administration Climate Program Office, and by the NOAA Physical Sciences  
Laboratory.

## References

- 475 Ajtić, J., Djurdjevic, V., Sarvan, D., Brattich, E., and Hernández-Ceballos, M.A.: Analysis of extreme beryllium-7  
specific activities in surface air, *Radiation & Applications*, 1(3), 216–221, doi:10.21175/RadJ.2016.03.040, 2016.  
Ajtić, J. V., Sarvan D., Djurdjevic, V. S., Hernández-Ceballos, M. A., and Brattich, E.: Beryllium-7 surface  
concentration extremes in Europe, *Facta Universitatis – Series: Physics, Chemistry and Technology*, 15 (1), 45–  
55, 2017.
- 480 Ajtić, J., Brattich, E., Sarvan, D., Djurdjevic, V., and Hernández-Ceballos, M. A.: Factors affecting the <sup>7</sup>Be surface  
concentration and its extremely high occurrences over the Scandinavian Peninsula during autumn and winter,  
*Chemosphere*, 199, 278–285, doi:10.1016/j.chemosphere.2018.02.052, 2018.
- Baldwin, M.P., and Dunkerton, T. J.: Stratospheric Harbingers of Anomalous Weather Regimes, *Science*, 294,  
581–584, doi:10.1126/science.1063315, 2001.
- 485 Bey, I., Jacob, D. J., Yantosca, R. M., Logan, J. A., Field, B. D., Fiore, A. M., Li, Q. B., Liu, H. G. Y., Mickley, L.  
J. and Schultz, M. G.: Global modeling of tropospheric chemistry with assimilated meteorology: Model description  
and evaluation, *J. Geophys. Res. Atmos.*, 106(D19), 23073–23095, doi:10.1029/2001JD000807, 2001.



- Bianchi, S., Plastino, W., Brattich, E., Djurdjevic, V., Longo, A., Hernández-Ceballos, M. A., Sarvan, D., and Ajtić, J.: Analysis of trends, periodicities, and correlations in the beryllium-7 time series in Northern Europe, *Appl. Radiat. Isot.* 148, 160-167, doi:10.1016/j.apradiso.2019.03.038, 2019.
- 490 Błażej, S., and Mietelski, J. W.: Cosmogenic  $^{22}\text{Na}$ ,  $^7\text{Be}$  and terrestrial  $^{137}\text{Cs}$ ,  $^{40}\text{K}$  radionuclides in ground level air samples collected weekly in Kraków (Poland) over years 2003–2006, *J. Radioanal. Nucl.*, 300, 747–756, doi:10.1007/s10967-014-3049-6, 2014.
- Brattich, E., Orza, J.A.G., Cristofanelli, P., Bonasoni, P., and Tositti, L.: Influence of stratospheric air masses on radiotracers and ozone over the central Mediterranean, *J. Geophys. Res.*, 122, doi:10.1002/2017JD027036, 2017a.
- 495 Brattich, E., Liu, H., Tositti, L., Considine, D. B., and Crawford, J. H.: Processes controlling the seasonal variations in  $^{210}\text{Pb}$  and  $^7\text{Be}$  at the Mt. Cimone WMO-GAW global station, Italy: a model analysis, *Atmos. Chem. Phys.*, 17(2), 1061-1080, doi:10.5194/acp-17-1061-2017, 2017b.
- Butler, A.H., Seidel, D. J., Hardiman, S. C., Butchart, N., Birner, T., and Match, A.: Defining Sudden Stratospheric Warmings, *Bull. Am. Meteorol. Soc.*, 96, 1913–1928, doi:10.1175/BAMS-D-13-00173.1, 2015.
- 500 Carruthers, D.J., Edmunds, H.A., Lester, A.E., McHugh, C.A., and Singles, R.J.: Use and validation of ADMS-Urban in contrasting urban and industrial locations, *Int. J. Environ. Pollut.*, 14, 363-374, doi:10.1504/IJEP.2000.000558, 2000.
- Chae, J-S., and Kim, G.: Large seasonal variations in fine aerosol precipitation rates revealed using cosmogenic  $^7\text{Be}$  as a tracer, *Sci. Total Environ.*, 673, 1-6, doi:10.1016/j.scitotenv.2019.03.482, 2019.
- 505 Chang, J.C., and Hanna, S.R.: Air quality model performance evaluation, *Meteorol. Atmos. Phys.*, 87, 167-196, doi:10.1007/s00703-003-0070-7, 2004.
- Chen, D.: A monthly circulation climatology for Sweden and its application to a winter temperature case study, *Int. J. Climatol.*, 20, 1067-1076, doi:10.1002/1097-0088(200008)20:10<1067::AID-JOC528>3.0.CO;2-Q, 2000.
- 510 Cristofanelli, P., Bonasoni, P., Collins, W., Feichter, J., Forster, C., James, P., Kentarchos, A., Kubik, P.W., Land, C., Meloan, J., Roelofs, G.J., Siegmund, P., Sprenger, M., Schnabel, C., Stohl, A., Tobler, L., Tositti, L., Trickl, T., and Zanis, P.: Stratosphere-to-troposphere transport: A model and method evaluation, *J. Geophys. Res. Atmos.*, 108 (12), doi:10.1029/2002JD002600, 2003.
- Cristofanelli, P., Bonasoni, P., Tositti, L., Bonafè, U., Calzolari, F., Evangelisti, F., Sandrini, S., and Stohl, A.: A 6-year analysis of stratospheric intrusions and their influence on ozone at Mt. Cimone (2165 m above sea level), *J. Geophys. Res. Atmos.*, 111, doi: 10.1029/2005JD006553, 2006
- 515



- Cristofanelli, P., Calzolari, F., Bonafé, U., Duchi, R., Marinoni, A., Roccatò, F., Tositti, L., and Bonasoni, P.: Stratospheric intrusion index (SI2) from baseline measurement data, *Theor. Appl. Climatol.*, 97, 317-325, doi: 10.1007/s00704-008-0073-x, 2009.
- 520 Cristofanelli, P., Brattich, E., Decesari, S., Landi, T.C., Maione, M., Putero, D., Tositti, L., and Bonasoni, P.: Studies on environmental radionuclides at Mt. Cimone, Chapter in: *High Mountain Atmospheric Research. The Italian Mt. Cimone WMO/GAW Global Station (2165 m a.s.l.)*, SpringerBriefs in Meteorology, Springer International Publishing, ISBN: 978-3-319-61126-6, doi: 10.1007/978-3-319-61127-3, 2018.
- De Cort, M., Sangiorgi, M. Hernandez Ceballos, M. A., Vanzo, S., Nweke, E., Tognoli, P. V., Tollefsen, T.: REM
- 525 data bank - Years 1984-2006. European Commission, Joint Research Centre (JRC) [Dataset] doi:10.2905/jrc-10117-10024 PID: <http://data.europa.eu/89h/jrc-10117-10024>, 2007
- Denton, M.H., Kivi, R., Ulich, T., Rodger, C.J., Clilverd, M.A., Denton, J.S., and Lester, M.: Observed response of stratospheric and mesospheric composition to sudden stratospheric warmings. *J. Atmos. Sol.*, 191, 105054, doi: 10.1016/j.jastp.2019.06.001, 2019.
- 530 Dutkiewicz, V.A., and Husain, L.: Stratospheric and tropospheric components of  $^7\text{Be}$  in surface air, *J. Geophys. Res. Atmos.*, 90, D3, 5783-5788, doi:10.1029/JD090iD03p05783, 1985.
- Eastham, S. D., Weisenstein, D. K. and Barrett, S. R. H.: Development and evaluation of the unified tropospheric-stratospheric chemistry extension (UCX) for the global chemistry-transport model GEOS-Chem, *Atmos. Environ.*, 89, 52–63, doi:10.1016/j.atmosenv.2014.02.001, 2014.
- 535 Engel, A., Möbius, T., Haase, H.-P., Bönisch, H., Wetter, T., Schmidt, U., Levin, I., Reddman, T., Oelhaf, H., Wetzell, G., Grunow, K., Huret, N., Pirre, M., 2006. Observation of mesospheric air inside the arctic stratosphere polar vortex in early 2003. *Atmos. Chem. Phys.*, 6, 267-282, doi:10.5194/acp-6-267-2006
- European Commission, 2000. Commission recommendation of 8 June 2000 on the application of Article 36 of the Euratom Treaty concerning the monitoring of the levels of radioactivity in the environment for the purpose of
- 540 assessing the exposure of the population as a whole. Available at <https://op.europa.eu/it/publication-detail/-/publication/8116b329-eb85-4bda-8d4b-e8c9e0d152c2/language-en>, last accessed 20 October 2020
- European Union (EU): Treaty Establishing the European Atomic Energy Community (E.A.E.C. – EURATOM), Consolidated Version, Title Two - Provisions for the Encouragement of the Progress in the Field of Nuclear Energy, Chapter III: Health and Safety, 2010.
- 545 Feely, H.W., Larsen, R. J., and Sanderson, C. G.: Factors that cause seasonal variations in beryllium-7 concentrations in surface air, *J. Environ. Radioact.*, 9, 223–249, doi:10.1016/0265-931X(89)90046-5, 1989.



- Gaffney, J.S., Marley, N., and Cunningham, M.M.: Natural radionuclides in fine aerosols in the Pittsburgh area. *Atmos. Environ.*, 38, 3191–3200, doi:10.1016/j.atmosenv.2004.03.015, 2004.
- 550 Gelaro, R., McCarthy, W., Suárez, M.J., Todling, R., Molod, A., Takacs, L., Randles, C.A., Darmenov, A., Bosilovich, M.G., Reichle, R., Wargan, K., Coy, L., Cullather, R., Draper, C., Akella, S., Buchard, V., Conaty, A., da Silva, A.M., Gu, W., Kim, G.-K., Koster, R., Lucchesi, R., Merkova, D., Nielsen, J.E., Partyka, G., Pawson, S., Putman, W., Rienecker, M., Schubert, S. D., Sienkiewicz, M., and Zhao, B.: The Modern-Era Retrospective Analysis for Research and Applications, Version 2 (MERRA-2), *J. Clim.*, 30(14), 5419–5454, doi:10.1175/JCLI-D-16-0758.1, 2017.
- 555 Gerasopoulos, E., Zanis, P., Stohl, A., Zerefos, C. S., Papastefanou, C., Ringer, W., Tobler, L., Hübener, S., Gäggeler, H. W., Kanter, H. J., Tositti, L., and Sandrini, S.: A climatology of  $^7\text{Be}$  at four high-altitude stations at the Alps and the Northern Apennines, *Atmos. Environ.*, 35, 6347–6360, doi :10.1016/S1352-2310(01)00400-9, 2001.
- Gerasopoulos, E., Zerefos, C. S., Papastefanou, C., Zanis, P., and O’Brien, K.: Low-frequency variability of beryllium-7 surface concentrations over the Eastern Mediterranean, *Atmos. Environ.*, 37, 1745–1756, doi:10-1016/S13552-2310(03)00068-2, 2003.
- 560 Gourdin, E., Evrard, O., Huon, S., Reyss, J.-L., Ribolzi, O., Bariac, T., Sengtaheuanghoung, O., and Ayrault, S.: Spatial and temporal variability of  $^7\text{Be}$  and  $^{210}\text{Pb}$  wet deposition during four successive monsoon storms in a catchment of northern Laos, *J. Environ. Radioact.*, 136, 195–205, doi:10.1016/j.jenvrad.2014.06.008, 2014.
- 565 Günther, G., Müller, R., von Hobe, M., Stroh, F., Konopka, P., and Volk, C. M.: Quantification of transport across the boundary of the lower stratospheric vortex during Arctic winter 2002/2003, *Atmos. Chem. Phys.*, 8, 3655–3670, doi:10.5194/acp-8-3655-2008, 2008.
- Hanna, S.R.: Uncertainties in air quality model predictions, *Bound.-Layer Meteorol.*, 62, 3–20, 1993.
- Hernández-Ceballos, M.A., Cinelli, G., Marín Ferrer, M., Tollefsen, T., De Felice, L., Nweke, E., Tognoli, P. V., 570 Vanzo, S., and De Cort, M.: A climatology of  $^7\text{Be}$  in surface air in European Union, *J. Environ. Radioact.*, 141, 62–70, doi:10.1016/j.jenvrad.2014.12.003, 2015.
- Hernández-Ceballos, M.A., Brattich, E., Cinelli, G., Ajtić, J., and Djurdjevic, V. Seasonality of  $^7\text{Be}$  concentrations in Europe and influence of tropopause height, *Tellus B*, 68, 29534, 2016.
- Hernández-Ceballos, M.A., Brattich, E., Lozano, R. L., and Cinelli, G.:  $^7\text{Be}$  behaviour and meteorological 575 conditions associated with  $^7\text{Be}$  peak events in Spain, *J. Environ. Radioact.*, 166, 17–26, doi:10.1016/j.jenvrad.2016.03.019, 2017



- Hsu, C.-P.F.: Air Parcel Motions during a Numerically Simulated Sudden Stratospheric Warming, *J. Atmos. Sci.*, 37, 2768–2792, doi:10.1175/1520-0469(1980)037<2768:APMDAN>2.0.CO;2, 1980.
- Huret, N., Pirre, M., Hauchecorne, A., Robert, C., Catoire, V., 2006. On the vertical structure of the stratosphere at midlatitudes during the first stage of the polar vortex formation and in the polar region in the presence of a large mesospheric descent. *J. Geophys. Res.* 111(D6), doi:10.1029/2005JD006102
- Ioannidou, A., and Papastefanou, C.: Precipitation scavenging of  $^7\text{Be}$  and  $^{137}\text{Cs}$  radionuclides in air, *J. Environ. Radioactiv.*, 85, 121–136, doi:10.1016/j.jenvrad.2005.06.005, 2006.
- Jacob, D. J. D., Prather, M. J. M., Rasch, P. P. J., Shia, R. R.-L., Balkanski, Y. J., Beagley, S. R., Bergmann, D. J., Blackshear, W. T., Brown, M., Chiba, M., Chipperfield, M.P., de Grandpré, J., Dignon, J.E., Feichter, J., Genthon, C., Grose, W.L., Kasibhatla, P.S., Köhler, I., Kritz, M.A., Law, K., Penner, J.E., Ramonet, M., Reeves, C.E., Rotman, D.A., Stockwell, D.Z., Van Velthoven, P.F.J., Verver, G., Wild, O., Yang H., and Zimmermann, P.: Evaluation and intercomparison of global atmospheric transport models using  $^{222}\text{Rn}$  and other short-lived tracers, *J. Geophys. Res. Atmos.*, 102(D5), 5953–5970, doi:10.1029/96JD02955, 1997.
- Jorba, O., Pérez, C., Rocadenbosch, F., and Baldasano, J.M. Cluster analysis of 4-day back trajectories arriving in the Barcelona area, Spain, from 1997 to 2002, *J. Appl. Meteorol. Climatol.*, 43,887–901, doi:10.1175/1520-0450(2004)043<0887:CAOBDT>2.0.CO;2, 2004.
- Kivi, R., Kyrö, E., Turunen, T., Harris, N.R.P., von der Gathen, P., Rex, M., Anderson, S.B., and Wohltmann, I.: Ozonesonde observations in the Arctic during 1989–2003: ozone variability and trends in the lower stratosphere and free troposphere, *J. Geophys. Res.*, 112, p. D08306, doi:10.1029/2006JD007271, 2007.
- Koch, D.M., Jacob, D.J., and Graustein, W.C.: Vertical transport in tropospheric aerosols as indicated by  $^7\text{Be}$  and  $^{210}\text{Pb}$  in a chemical tracer model, *J. Geophys. Res. Atmos.*, 101, 18651–18666, doi:10.1029/96JD01176, 1996.
- Lal, D., and Peters, B.: Cosmic ray produced radioactivity on the earth, in: Sitte, K. (Ed.), *Cosmic Rays II*. Springer Berlin Heidelberg, pp. 551–612, 1967.
- Lee, H.N., Tositti, L., Zheng, X., and Bonasoni, P.: Analyses and comparisons of  $^7\text{Be}$ ,  $^{210}\text{Pb}$  and activity ratio  $^7\text{Be}/^{210}\text{Pb}$  with ozone observations at two GAW stations from high mountains, *J. Geophys. Res. Atmos.*, 112, 1–11, doi: 10.1029/2006JD007421, 2007.
- Leppänen, A.-P.: Deposition of naturally occurring  $^7\text{Be}$  and  $^{210}\text{Pb}$  in Northern Finland, *J. Environ. Radioactiv.*, 208–209, 105995, doi:10.1016/j.jenvrad.2019.105995, 2019.
- Leppänen, A.-P., Pacini, A.A., Usoskin, I.G., Aldahan, A., Echer, E., Evangelista, H., Klemola, S., Kovaltsov, G.A., Mursula, K., and Possnert, G.: Cosmogenic  $^7\text{Be}$  in air: a complex mixture of production and transport, *J. Atmos. Sol.*, 72, 1036–1043, doi:10.1016/j.jastp.2010.06.006, 2010.





- Limpasuvan, V., Thompson, D. W. J., Hartmann, D. L.: The Life Cycle of the Northern Hemisphere Sudden Stratospheric Warmings. *J. Clim.*, 17, 2584–2596, doi:10.1175/1520-0442(2004)017<2584:TLCOTN>2.0.CO;2, 610 2004
- Lin, J. T., and McElroy, M. B.: Impacts of boundary layer mixing on pollutant vertical profiles in the lower troposphere: Implications to satellite remote sensing, *Atmos. Environ.*, 44(14), 1726–1739, doi:10.1016/j.atmosenv.2010.02.009, 2010.
- Lin, S.-J. and Rood, R. B.: Multidimensional Flux-Form Semi-Lagrangian Transport Schemes, *Mon. Weather Rev.*, 615 124(9), 2046–2070, doi:10.1175/1520-0493(1996)124<2046:MFFSLT>2.0.CO;2, 1996.
- Linderson, M.-L.: Objective classification of atmospheric circulation over Southern Scandinavia, *Int. J. Climatol.*, 21, 155-169, doi:10.1002/joc.604, 2001.
- Liu, H., Jacob, D. J., Bey, I. and Yantosca, R. M.: Constraints from  $^{210}\text{Pb}$  and  $^7\text{Be}$  on wet deposition and transport in a global three-dimensional chemical tracer model driven by assimilated meteorological fields, *J. Geophys. Res.* 620 *Atmos.*, 106(D11), 12109–12128, doi:10.1029/2000JD900839, 2001.
- Liu, H., Considine, D. B., Horowitz, L. W., Crawford, J. H., Rodriguez, J. M., Strahan, S. E., Damon, M. R., Steenrod, S. D., Xu, X., Kouatchou, J., Carouge, C., and Yantosca, R. M.: Using beryllium-7 to assess cross-tropopause transport in global models, *Atmos. Chem. Phys.*, 16, 4641–4659, doi:10.5194/acp-16-4641-2016, 2016.
- Mari, C., Jacob, D. J. and Bechtold, P.: Transport and scavenging of soluble gases in a deep convective cloud, *J.* 625 *Geophys. Res. Atmos.*, 105(D17), 22255–22267, doi:10.1029/2000JD900211, 2000.
- Mattsson, R., Paatero, J., and Hatakka, J.: Automatic Alpha/Beta Analyser for Air Filter Samples - Absolute Determination of Radon Progeny by Pseudo-coincidence Techniques, *Radiat. Prot. Dosim.*, 63, 133-139, doi:10.1093/oxfordjournals.rpd.a031520, 1996.
- Mitchell, D.M., Gray, L.J., and Anstey, J.: The influence of stratospheric vortex displacements and splits on surface 630 climate, *J. Clim.*, 26, 2668-2682, doi:10.1175/JCLI-D-12-00030.1, 2013.
- Müller, M., Neuber, R., Fierli, F., Hauchecorne, A., Vömel, H., and Oltmans, S. J.: Stratospheric water vapour as tracer for vortex filamentation in the Arctic winter 2002/2003, *Atmos. Chem. Phys.*, 3, 4393–4410, doi:10.5194/acp-3-1991-2003, 2003.
- Müller, R., Tilmes, S., Groß, J.-U., Engel, A., Oelhaf, H., Wetzell, G., Huret, N., Pirre, M., Catoire, V., Toon, G., 635 Nakjima, H., 2007. Impact of mesospheric intrusions on ozone-tracer relations in the stratospheric polar vortex. *J. Geophys. Res.*, 112(D23), doi:10.1029/2006JD008315
- NCEP/NWS/NOAA/U.S. Department of Commerce: NCEP FNL Operational Model Global Tropospheric Analyses, continuing from July 1999. Research Data Archive at the National Center for Atmospheric Research.





- Computational and Information Systems Laboratory, doi:10.5065/D6M043C6, Updated daily, Accessed October  
640 2020
- O'Brien, K.: Secular variations in the production of cosmogenic isotopes in the earth's atmosphere. *J. Geophys. Res.*, 84, 423-431, doi:10.1029/JA084iA02p00423, 1979.
- Paatero, J., Hatakka, J., and Viisanen, Y.: Trajectory Analysis of  $^{210}\text{Pb}$  and  $^7\text{Be}$  in Ground-Level Air in Southern Finland. *Radiochemistry*, 43, 475–481, doi:10.1023/A:1013069206962, 2001.
- 645 Pacini, A.A., Usoskin, I. G., Mursula, K., Echer, E., and Evangelista, H.: Signature of a sudden stratospheric warming in the near-ground  $^7\text{Be}$  flux, *Atmos. Environ.*, 113, 27–31, doi:10.1016/j.atmosenv.2015.04.065, 2015.
- Park, R. J., Jacob, D. J., Field, B. D., Yantosca, R. M. and Chin, M.: Natural and transboundary pollution influences on sulfate-nitrate-ammonium aerosols in the United States: Implications for policy, *J. Geophys. Res. Atmos.*, 109(15), doi:10.1029/2003JD00473, 2004.
- 650 Peethani, S., Sharma, N., and Pathakoti, M.: Effect of tropospheric and stratospheric temperatures on tropopause height, *Remote Sens. Lett.*, 5, 11, 933-940, doi:10.1080/2150704X.2014.973078, 2014.
- Peters, D.H.W., Vargin, P., Gabriel, A., Tsvetkova, N., and Yushkov, V.: Tropospheric forcing of the boreal polar vortex splitting in January 2003, *Annales Geophysicae*, 28, 2133–2148, doi:10.5194/angeo-28-2133-2010, 2010.
- Piñero García, F., Ferro García, M. A., and Azahra, M.:  $^7\text{Be}$  behaviour in the atmosphere of the city of Granada  
655 January 2005 to December 2009, *Atmos. Environ.*, 47, 84–91, doi:10.1016/j.atmosenv.2011.11.034, 2012.
- Putero, D., Cristofanelli, P., Sprenger, M., Škerlak, B., Tositti, L., and Bonasoni, P.: STEFLUX, a tool for investigating stratospheric intrusions: application to two WMO/GAW global stations, *Atmos. Chem. Phys.*, 16, 14203-14217, doi: [10.5194/acp-16-14203-2016](https://doi.org/10.5194/acp-16-14203-2016), 2016
- Salminen-Paatero, S., Thölix, L., Kivi, R., and Paatero, J.: Nuclear contamination sources in surface air of Finnish  
660 Lapland in 1965–2011 studied by means of  $^{137}\text{Cs}$ ,  $^{90}\text{Sr}$ , and total beta activity, *Environ. Sci. Pollut. Res.*, 26, 21511–21523, doi:10.1007/s11356-019-05451-0, 2019.
- Salvador, P., Artíñano, B., Querol, X., Alastuey, A.: A combined analysis of backward trajectories and aerosol chemistry to characterise long-range transport episodes of particulate matter: The Madrid air basin, a case study, *Sci Tot Environ.*, 390, 495-506, doi:10.1016/j.scitotenv.2007.10.052, 2008.
- 665 Sangiorgi, M., Hernández Ceballos, M.A., Iurlaro, G., Cinelli, G., and De Cort, M.: 30 years of European Commission Radioactivity Environmental Monitoring data bank (REMdb) – an open door to boost environmental radioactivity research. *Earth Sys. Sci. Data*, 11, 589-601, doi:10.5194/essd-11-589-2019, 2019.



- Stein, A.F., Draxler, R.R., Rolph, G.D., Stunder, B.J.B., Cohen, M.D., and Ngan, F.: NOAA's HYSPLIT atmospheric transport and dispersion modeling system, *Bull. Am. Meteorol. Soc.*, 96, 2059-2077, doi:10.1175/BAMS-D-14-00110.1, 2015.
- 670 Sýkora, I., Holý, K., Jeskovský, M., Müllerová, M., Bulko, M., and Povinec, P. P.: Long-term variations of radionuclides in the Bratislava air, *J. Environ. Radioactiv.*, 166, 27–35, doi:10.1016/j.jenvrad.2016.03.004, 2017.
- Terzi, L., and Kalinowski, M. B.: World-wide seasonal variation of  $^7\text{Be}$  related to large-scale atmospheric circulation dynamics, *J. Environ. Radioactiv.*, 178-179, 1–15, doi:10.1016/j.jenvrad.2017.06.031, 2017.
- 675 Tilmes, S., Müller, R., Engel, A., Rex, M., Russell III, J.M., 2006. Chemical ozone loss in the Arctic and Antarctic stratosphere between 1992 and 2005. *Geophys. Res. Lett.* 33(20), doi:10.1029/2006GL026925
- Tositti, L., Hübener, S., Kanter, H.J., Ringer, W., Sandrini, S., and Tobler, L.: Intercomparison of sampling and measurement of  $^7\text{Be}$  in air at four high-altitude locations in Europe, *Appl. Rad. Isot.*, 61, 1497-1502, doi:10.1016/j.apradiso.2004.04.003, 2004.
- 680 Tositti, L., Hübener, S., Kanter, H.J., Ringer, W., Sandrini, S., and Tobler, L.: Intercomparison of sampling and measurement of  $^7\text{Be}$  in air at four high-altitude locations in Europe. *Appl. Radiat. Isot.*, 61(6), 1497-1502, doi:10.1016/j.apradiso.2004.04.003
- Tositti, L., Brattich, E., Cinelli, G., and Baldacci, D.: 12 years of  $^7\text{Be}$  and  $^{210}\text{Pb}$  in Mt. Cimone and their correlation with meteorological parameters, *Atmos. Environ.*, 87, 108-122, doi: 10.1016/j.atmosenv.2014.01.014, 2014.
- 685 Wang, Q., Jacob, D. J., Fisher, J. A., Mao, J., Leibensperger, E. M., Carouge, C. C., Le Sager, P., Kondo, Y., Jimenez, J. L., Cubison, M. J., Doherty, S. J., Sager, P. Le, Kondo, Y., Jimenez, J. L., Cubison, M. J., and Doherty, S.J.: Sources of carbonaceous aerosols and deposited black carbon in the Arctic in winter-spring: implications for radiative forcing, *Atmos. Chem. Phys.*, 11(23), 12453–12473, doi:10.5194/acp-11-12453-2011, 2011, 2011.
- Wargan, K., and Coy, L.: Strengthening of the tropopause inversion layer during the 2009 Sudden Stratospheric Warming: a MERRA-2 study. *Journal of the Atmospheric Sciences*, 73(5), 1871-1887, doi:10.1175/JAS-D-15-0333.1
- 690 Waugh, D.W., Sobel, A.H., Polvani, L.M., 2017. What is the polar vortex and how does it influence weather? *Bull. Am. Meteorol. Soc.*, 98, 37-44, doi:10.1175/BAMS-D-15-00212.1, 2016.
- Wesley, M. L.: Parameterization of surface resistance to gaseous dry deposition in regional numerical models, *Atmos. Environ.*, 16, 1293-1304, 1989.
- 695 Wu, S., Mickley, L. J., Jacob, D. J., Logan, J. A., Yantosca, R. M. and Rind, D. Why are there large differences between models in global budgets of tropospheric ozone? *J. Geophys. Res. Atmos.*, 112(D5), 1–18, doi:10.1029/2006JD007801, 2007.



- 700 Yu, K., Keller, C. A., Jacob, D. J., Molod, A. M., Eastham, S. D. and Long, M. S.: Errors and improvements in the  
use of archived meteorological data for chemical transport modeling: an analysis using GEOS-Chem v11-01 driven  
by GEOS-5 meteorology, *Geosci. Model Dev.*, 11, 305–319, doi:10.5194/gmd-2017-125, 2018.
- Zanis, P., Schuepbach, E., Gäggeler, H.W., Hübener, S., and Tobler, L.: Factors controlling beryllium-7 at  
Jungfraujoch in Switzerland, *Tellus*, 51 (4), 789e805, doi:10.1034/j.1600-0889.1999.t01-3-00004.x, 1999.
- 705 Zhang, B., H. Liu, J.H. Crawford, G. Chen, T.D. Fairlie, S. Chambers, C.-H. Kang, A.G. Williams, K. Zhang, D.B.  
Considine, M. P. Sulprizio, and R.M. Yantosca: Simulation of radon-222 with the GEOS-Chem global model:  
Emissions, seasonality, and convective transport, *Atmos. Chem. Phys. Discuss.*, in review, doi:10.5194/acp-2020-  
804, 2020.



## Tables

710 **Table 1.** (left) Normalized differences between the MERRA-2 and observed precipitation, calculated as differences between  
 the MERRA-2 and the observed values, normalized over the observed value, at each sampling site. Positive values indicate  
 that the model tends to overestimate observations while the negative ones indicate underestimation. (right) Statistical  
 parameters (mean  $\pm$  SD = standard deviation; MB = mean bias; NMSE = normalized mean square error; FA2 = factor of 2)  
 715 indicating the model performance in reproducing GPCP monthly accumulated precipitation at the six sampling sites in  
 Northern Europe.

Sampling site	Normalized differences			Statistical parameters				
	Jan-03	Feb-03	Mar-03	Mean $\pm$ SD (mm)		MB (mm)	NMSE	FA2
				MERRA-2	GPCP			
<b>Ivalo</b>	-0.07	0.63	1.25	2.23 $\pm$ 0.67	1.48 $\pm$ 0.43	0.75	0.34	1
<b>Umea</b>	-0.03	0.07	0.08	1.53 $\pm$ 0.86	1.53 $\pm$ 0.94	0.02	0	1
<b>Helsinki</b>	-0.09	-0.21	0.17	1.23 $\pm$ 0.92	1.32 $\pm$ 1.03	-0.09	0.01	1
<b>Kista</b>	0.96	-0.03	1.73	1.12 $\pm$ 0.92	0.67 $\pm$ 0.46	0.46	0.42	0.67
<b>Harku</b>	-0.2	0.18	-0.07	1.23 $\pm$ 0.92	1.42 $\pm$ 1.28	-0.18	0.05	1
<b>Risoe</b>	-0.06	2.45	1.52	1.63 $\pm$ 0.37	1.05 $\pm$ 0.98	0.58	0.3	0.33



720

725

**Table 2.** (left) Normalized differences between the simulated and observed  $^7\text{Be}$  monthly means, calculated as differences between the simulated and the observed values, normalized over the observed value, at each sampling site. (right) Statistical parameters (mean  $\pm$  SD = standard deviation; MB = mean bias; NMSE = Normalized Mean Square Error; FA2 = Factor of 2) indicating the model performance in reproducing observed  $^7\text{Be}$  monthly means at the six sampling sites in Northern Europe and  $^7\text{Be}/^{210}\text{Pb}$  and  $^{210}\text{Pb}$  monthly means in Helsinki.

Sampling Site	Tracer	Normalized differences			Statistical parameters				
		Jan-03	Feb-03	Mar-03	Mean $\pm$ SD		MB	NMSEFA2	
					Modelled	Observed			
Ivalo	$^7\text{Be}$	0.15	0.08	-0.07	(1.82 $\pm$ 0.49) mBq m <sup>-3</sup>	(1.85 $\pm$ 0.78) mBq m <sup>-3</sup>	-0.03 mBq m <sup>-3</sup>	0.07	1
Umea		-0.01	-0.14	-0.05	(1.69 $\pm$ 0.72) mBq m <sup>-3</sup>	(1.88 $\pm$ 0.96) mBq m <sup>-3</sup>	1.69 mBq m <sup>-3</sup>	0.89	1
Helsinki		-0.22	-0.31	-0.2	(1.58 $\pm$ 0.80) mBq m <sup>-3</sup>	(2.30 $\pm$ 0.60) mBq m <sup>-3</sup>	1.57 mBq m <sup>-3</sup>	0.76	0.74
Kista		-0.28	-0.35	-0.25	(1.68 $\pm$ 0.69) mBq m <sup>-3</sup>	(2.41 $\pm$ 0.89) mBq m <sup>-3</sup>	-0.73 mBq m <sup>-3</sup>	0.16	0.92
Harku		-0.21	-0.13	-0.28	(1.61 $\pm$ 0.61) mBq m <sup>-3</sup>	(2.16 $\pm$ 0.81) mBq m <sup>-3</sup>	-0.54 mBq m <sup>-3</sup>	0.17	0.93
Risoe		-0.32	-0.4	-0.08	(2.08 $\pm$ 0.83) mBq m <sup>-3</sup>	(3.31 $\pm$ 1.52) mBq m <sup>-3</sup>	2.08 mBq m <sup>-3</sup>	0.7	0.62
Helsinki	$^7\text{Be}/^{210}\text{Pb}$	-0.28	-0.5	-0.5	4.89 $\pm$ 3.57	10.4 $\pm$ 7.5	-5.04	0.78	0.45
Helsinki	$^{210}\text{Pb}$	0.73	0.5	0.66	(0.48 $\pm$ 0.29) mBq m <sup>-3</sup>	(0.36 $\pm$ 0.32) mBq m <sup>-3</sup>	0.12 mBq m <sup>-3</sup>	0.3	0.78

730



**Table 3.** Statistical parameters indicating the model performance in reproducing observed  $^7\text{Be}$  weekly (daily in the case of Helsinki) means at the six sampling sites in Northern Europe.

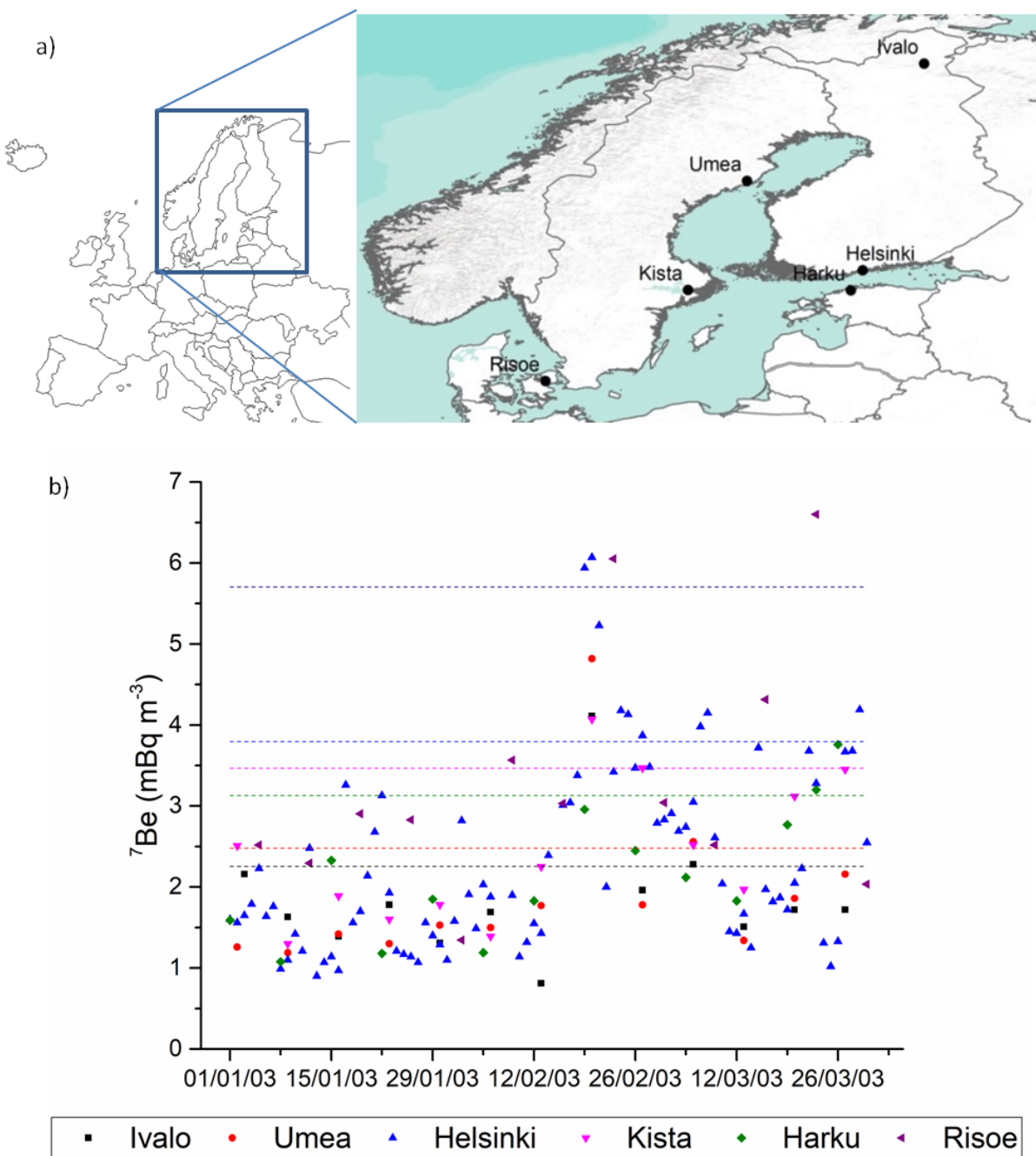
Sampling site	Tracer	Mean $\pm$ SD		MB	NMSE	R	FA2
		Modelled	Observed				
Ivalo	$^7\text{Be}$	(1.52 $\pm$ 0.44) mBq m <sup>-3</sup>	(1.85 $\pm$ 0.78) mBq m <sup>-3</sup>	-0.33 mBq m <sup>-3</sup>	0.12	0.74	1.00
Umea		(1.43 $\pm$ 0.72) mBq m <sup>-3</sup>	(1.88 $\pm$ 0.96) mBq m <sup>-3</sup>	-0.45 mBq m <sup>-3</sup>	0.11	0.91	0.92
Helsinki		(1.35 $\pm$ 0.83) mBq m <sup>-3</sup>	(2.30 $\pm$ 1.15) mBq m <sup>-3</sup>	-0.88 mBq m <sup>-3</sup>	0.47	0.64	0.57
Kista		(1.43 $\pm$ 0.62) mBq m <sup>-3</sup>	(2.41 $\pm$ 0.89) mBq m <sup>-3</sup>	-0.98 mBq m <sup>-3</sup>	0.30	0.86	0.62
Harku		(1.36 $\pm$ 0.56) mBq m <sup>-3</sup>	(2.16 $\pm$ 0.81) mBq m <sup>-3</sup>	-0.79 mBq m <sup>-3</sup>	-0.45	0.73	0.86
Risoe		(1.84 $\pm$ 0.89) mBq m <sup>-3</sup>	(3.31 $\pm$ 1.52) mBq m <sup>-3</sup>	-1.47 mBq m <sup>-3</sup>	0.77	0.10	0.38
Helsinki	$^7\text{Be}/^{210}\text{Pb}$	4.86 $\pm$ 3.96	10.3 $\pm$ 7.5	-5.06	0.85	0.66	0.43

735

740

745

## Figures



750 **Figure 1.** a) Location of the  $^7\text{Be}$  sampling sites in Northern Europe (source: <https://mapamundiparaimprimir.com/europa/>); b)  $^7\text{Be}$  concentrations measured at six surface sampling sites in Northern Europe during the 2002/2003 boreal winter. Dashed lines indicate the 90<sup>th</sup> percentile reference line for each sampling site.





## Total Precipitation, 2003

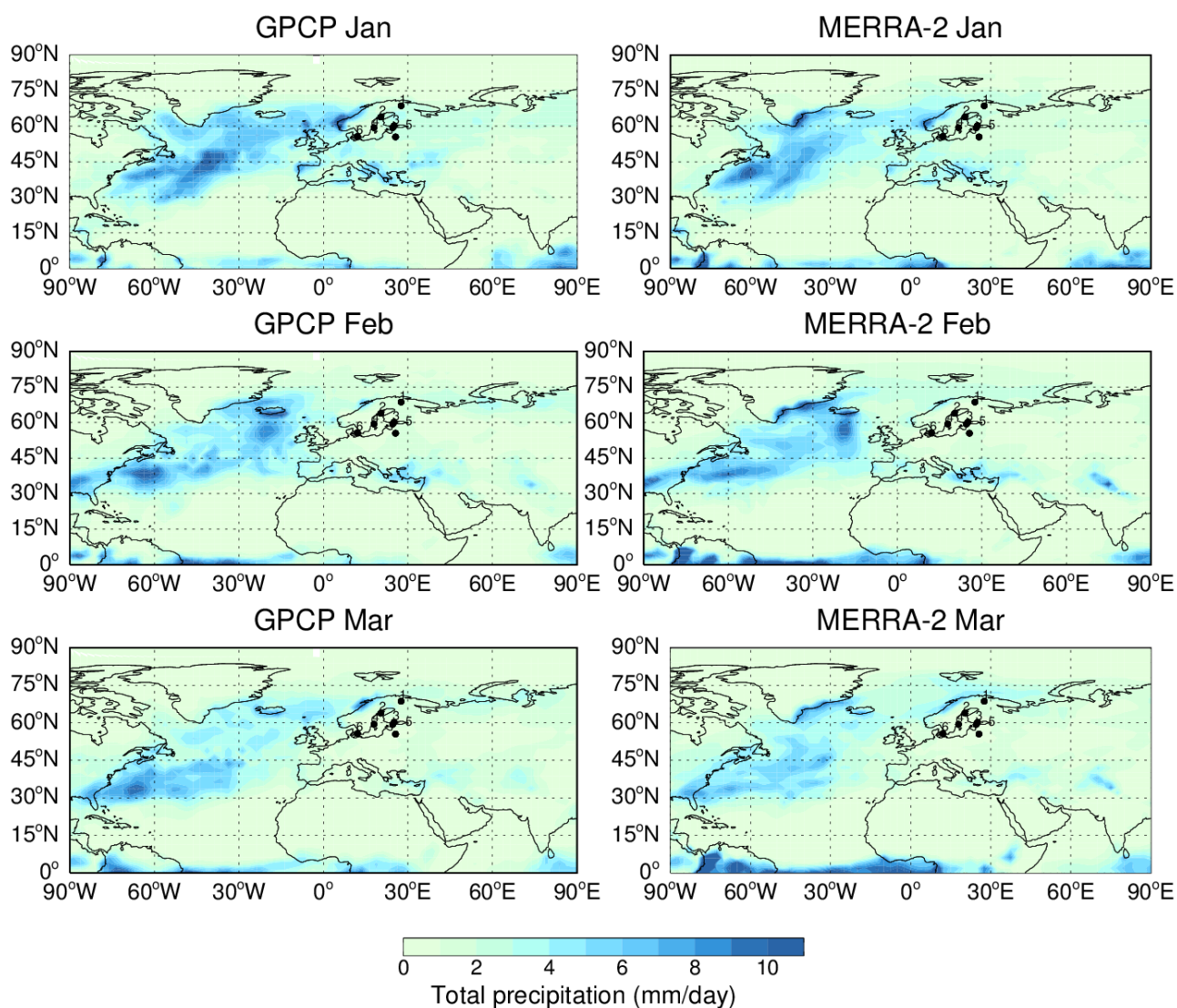


**Figure 2.** Comparison of the MERRA-2 total precipitation during January-March 2003 with the GPCP observations. The black dots indicate the locations of the sampling sites: 1=Ivalo, 2=Umea, 3= Helsinki, 4=Kista, 5=Harku, 6=Risoe.

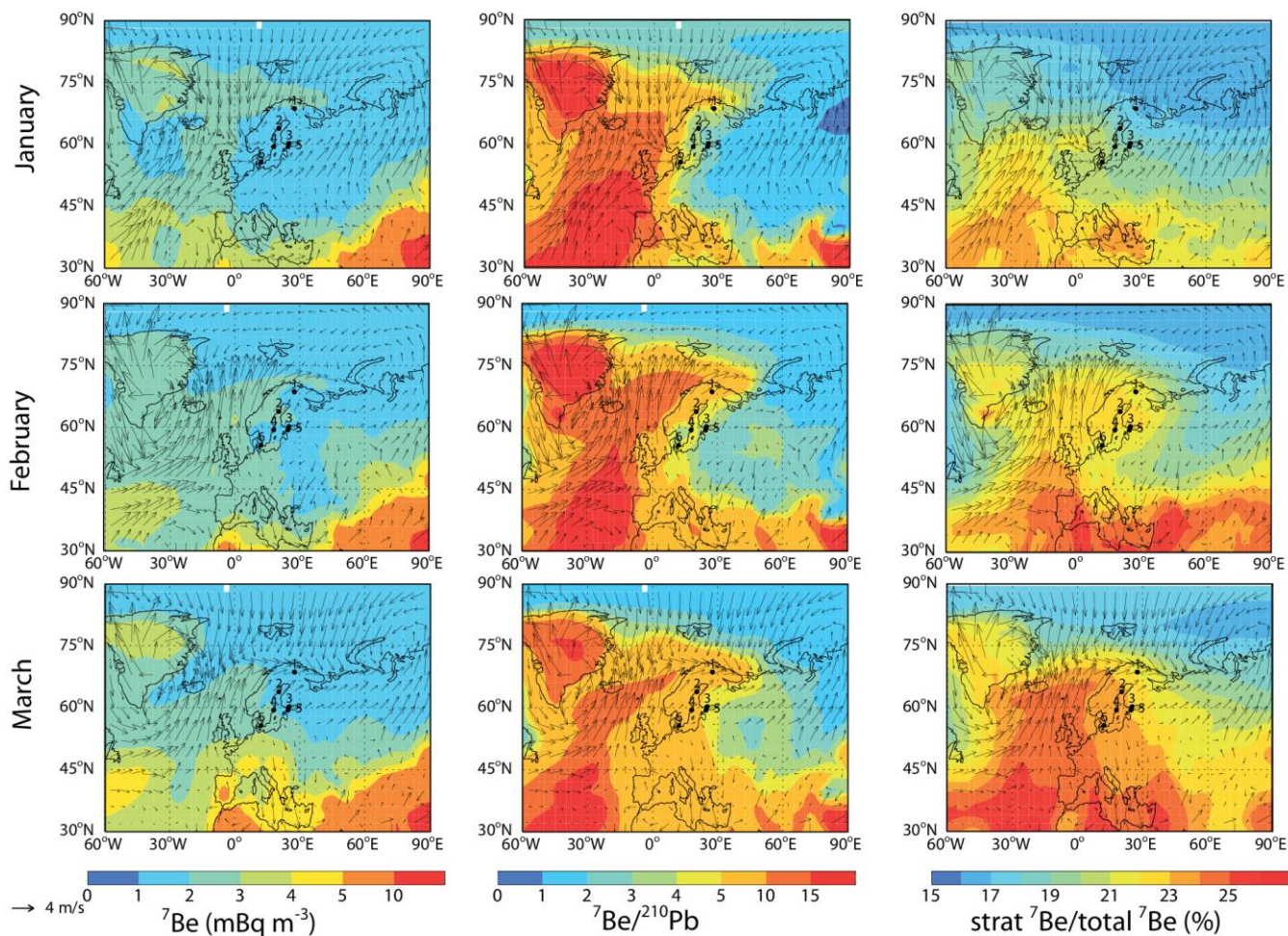


**Figure 3.** Simulated monthly mean  ${}^7\text{Be}$  surface concentrations ( $\text{mBq m}^{-3}$ ),  ${}^7\text{Be}/{}^{210}\text{Pb}$  ratio and fraction of stratospheric  ${}^7\text{Be}$ . Arrows represent winds in the MERRA-2 reanalysis. The dots indicate the locations of the sampling sites: 1=Ivalo, 2=Umea, 3=Helsinki, 4=Kista, 5=Harku, 6=Risoe.

760

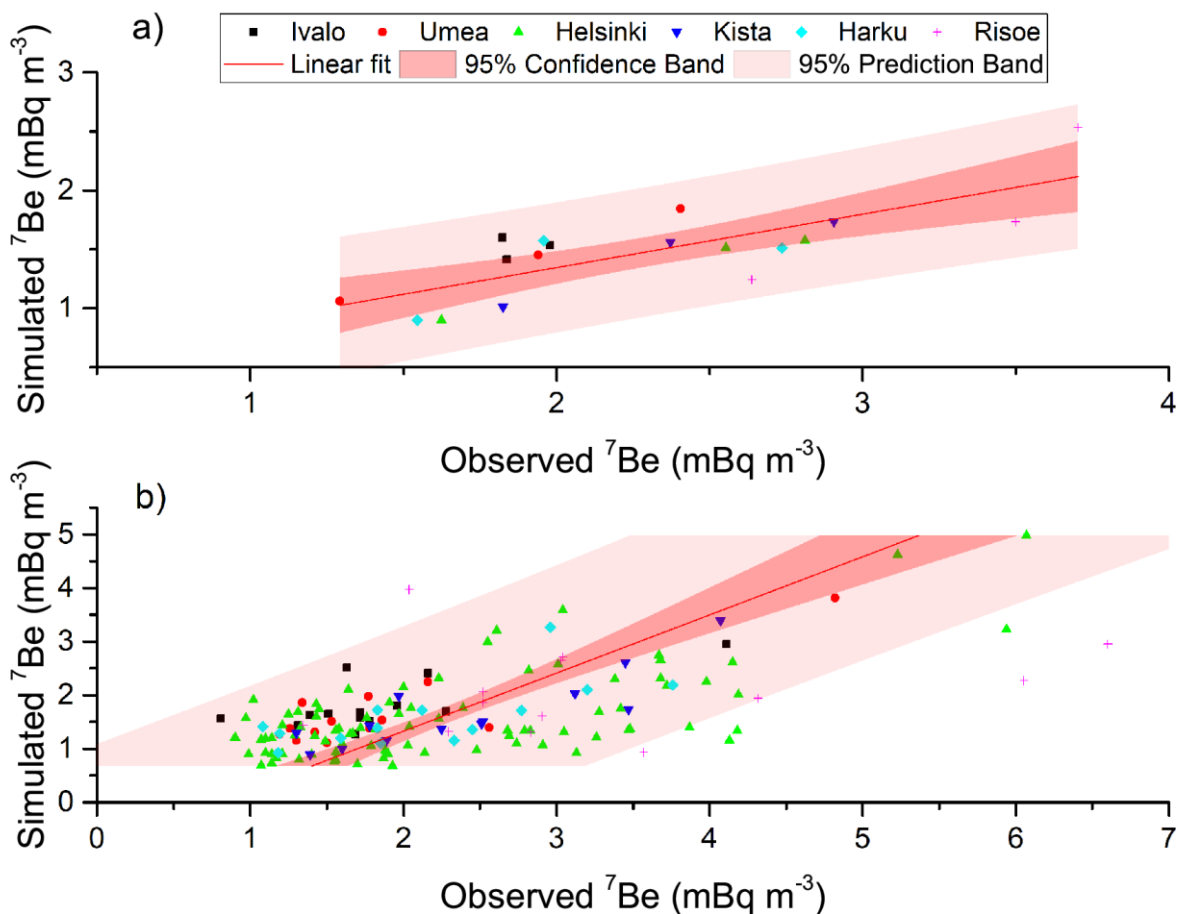
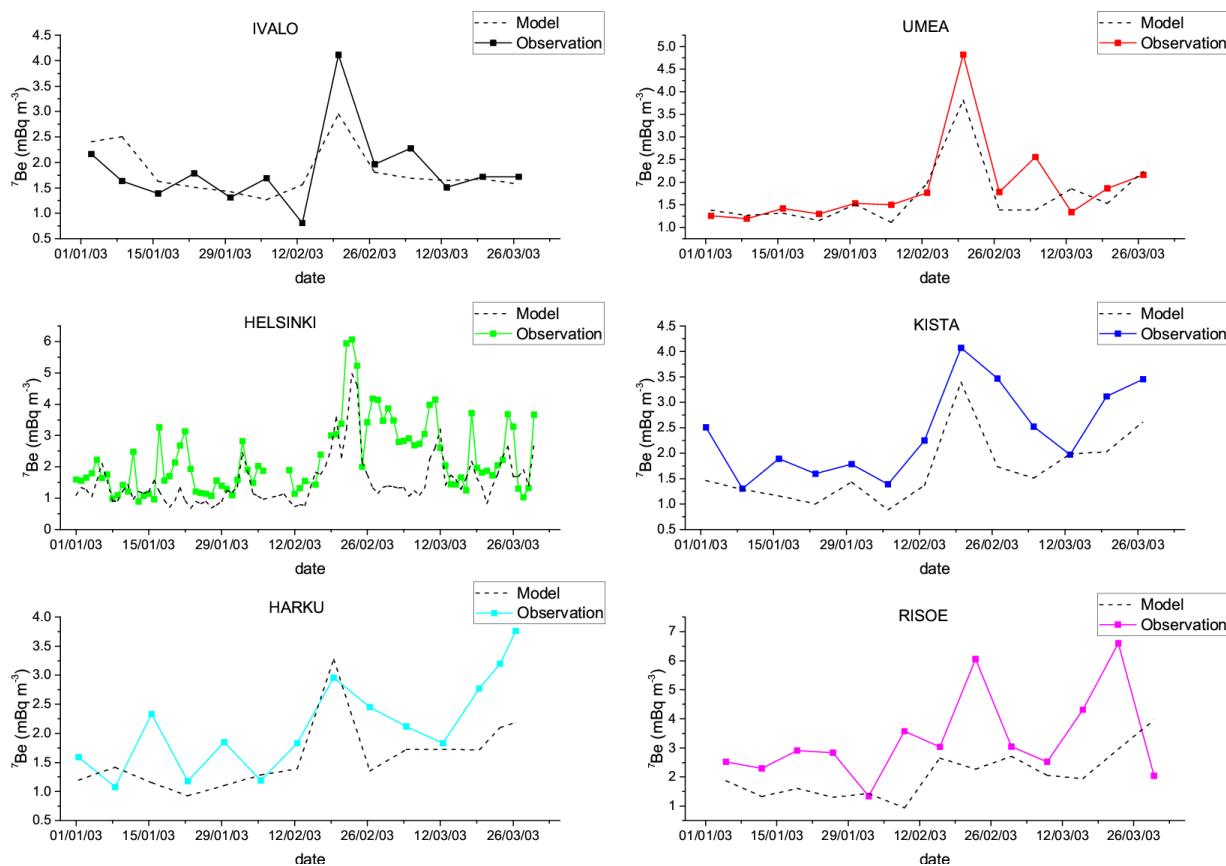


**Figure 4.** Scatter plots of: a) simulated vs. observed  ${}^7\text{Be}$  monthly means at the six sampling sites; b) simulated vs. observed  ${}^7\text{Be}$  weekly (daily in the case of Helsinki) means at the six sampling sites. Also shown are the linear fit and the 95% confidence and prediction bands around the linear fit.



770 **Figure 5.** Temporal evolution of simulated and observed  $^7\text{Be}$  surface concentrations at the six sampling sites. Values are weekly (daily in the case of Helsinki) means.



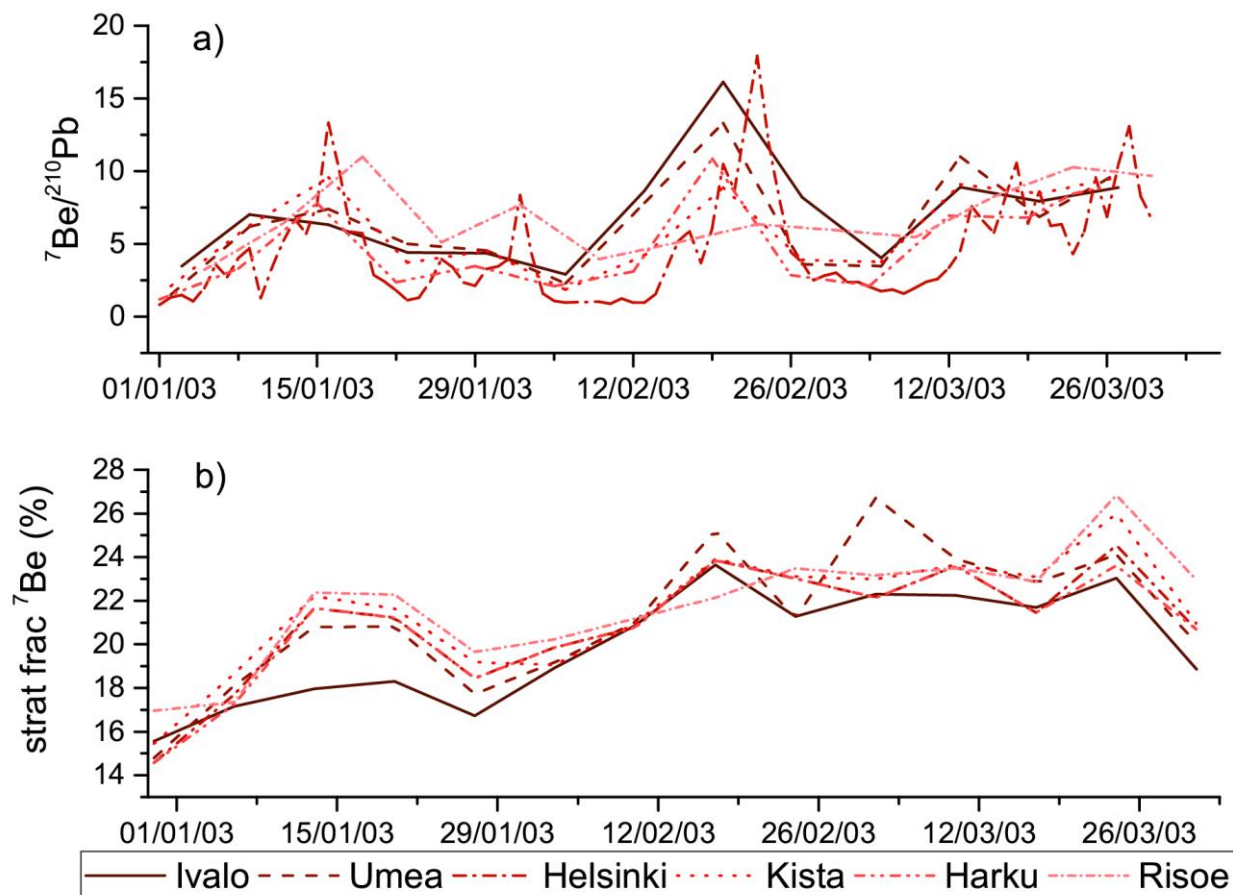
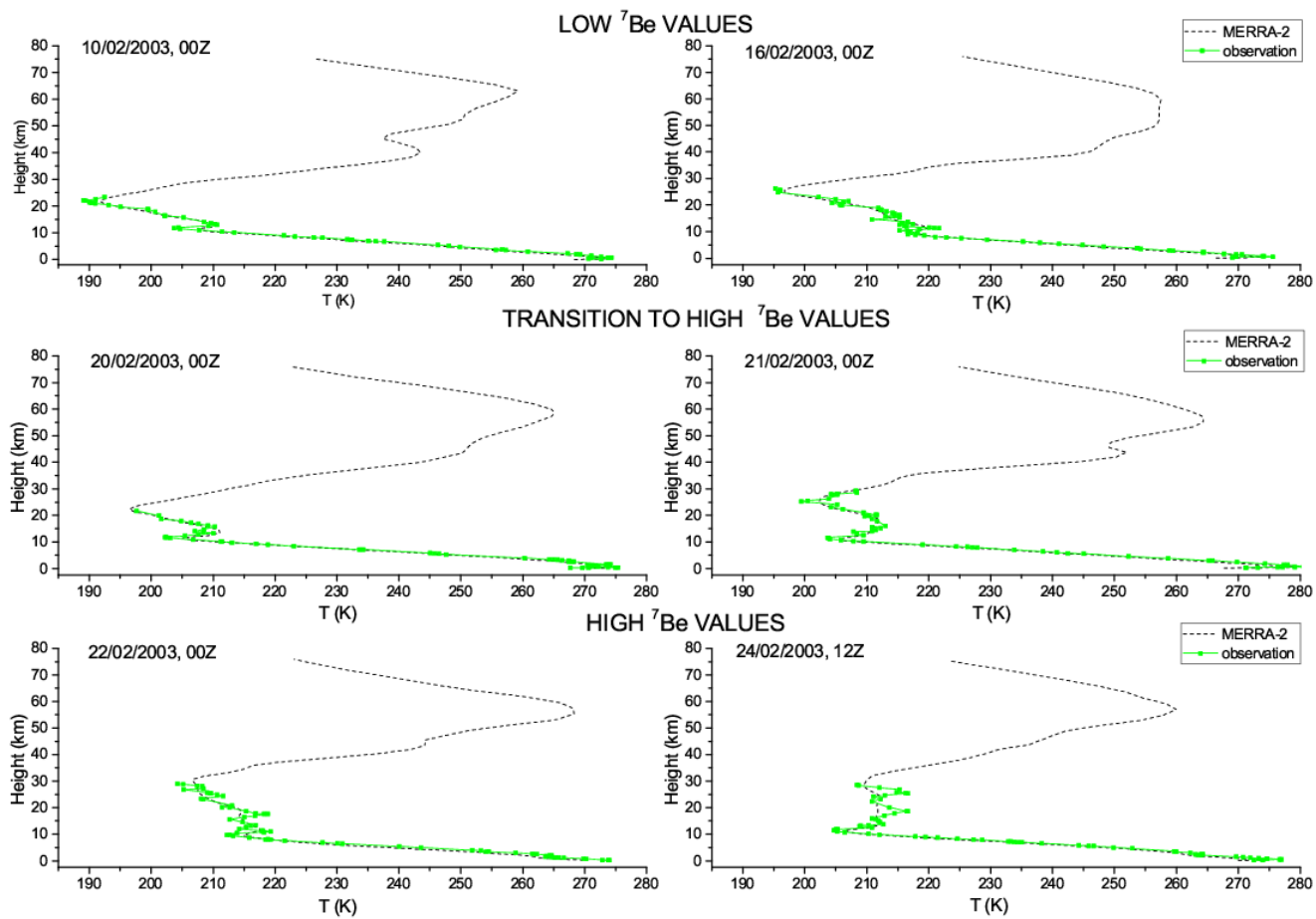


**Figure 6.** Temporal evolution of the simulated a)  ${}^7\text{Be}/{}^{210}\text{Pb}$  and b) fraction of stratospheric  ${}^7\text{Be}$  (calculated as the ratio between the stratospheric  ${}^7\text{Be}$  and the total  ${}^7\text{Be}$  concentrations, in percentage) at the six sampling sites during January-March 2003. Values are weekly means.

775



780

**Figure 7.** Vertical profiles of air temperature in the MERRA-2 reanalysis (dotted line) and in the soundings at the Sodankylä station in Finland on selected days of low <sup>7</sup>Be values (top panels: 10 and 16 Feb 2003, 00 UTC), transition to high <sup>7</sup>Be values (middle panels: 20 Feb 2003, 00 UTC and 21 Feb 2003, 12 UTC) and high <sup>7</sup>Be values (bottom panels: 22 and 24 Feb 2003, 00 UTC) at the six sampling sites in Northern Europe.

785

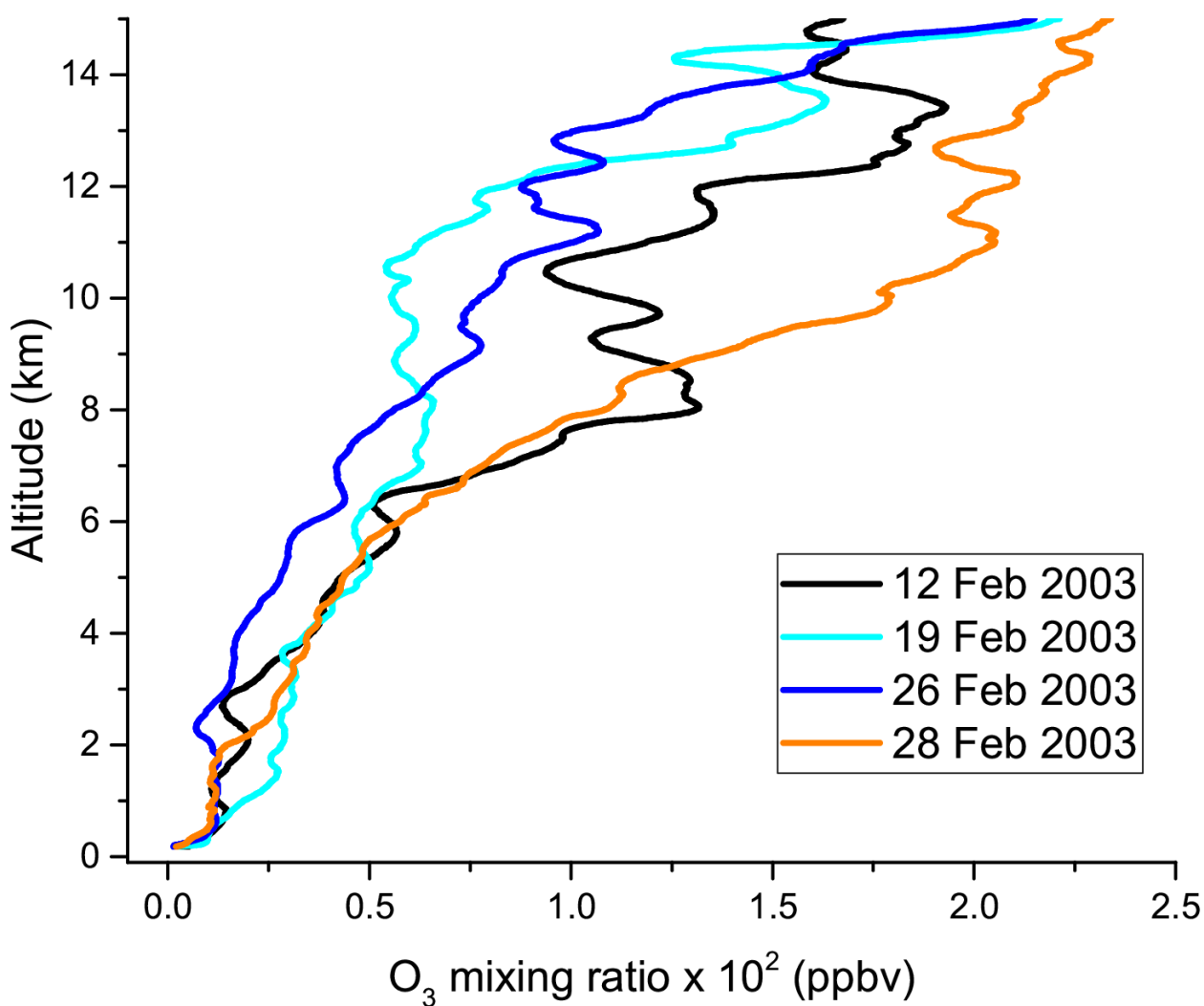


**Figure 8.** Ozone soundings at the Sodankylä Arctic station during 4 different days in February 2003: 12, 19, 16 and 28 February 2003.



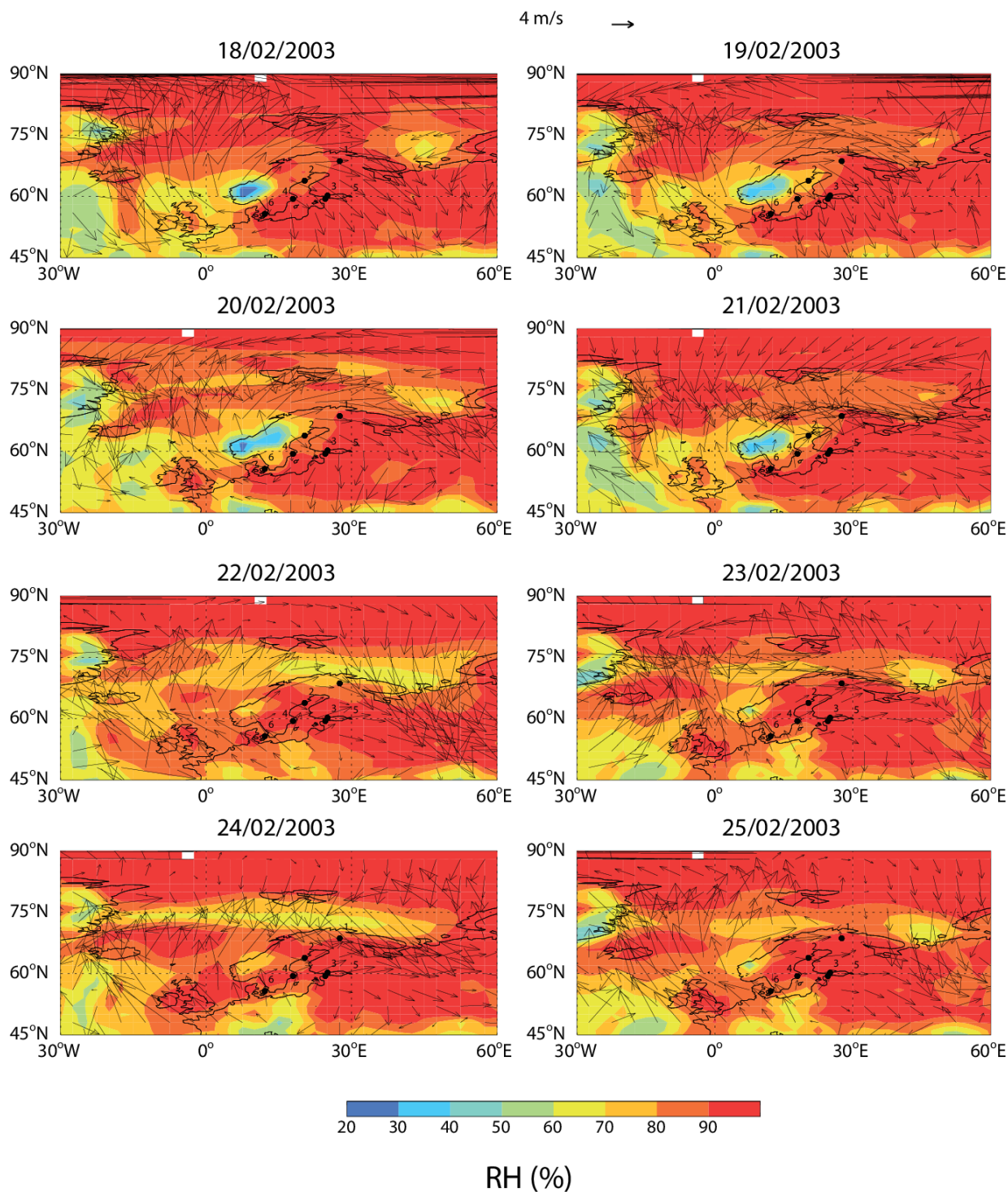
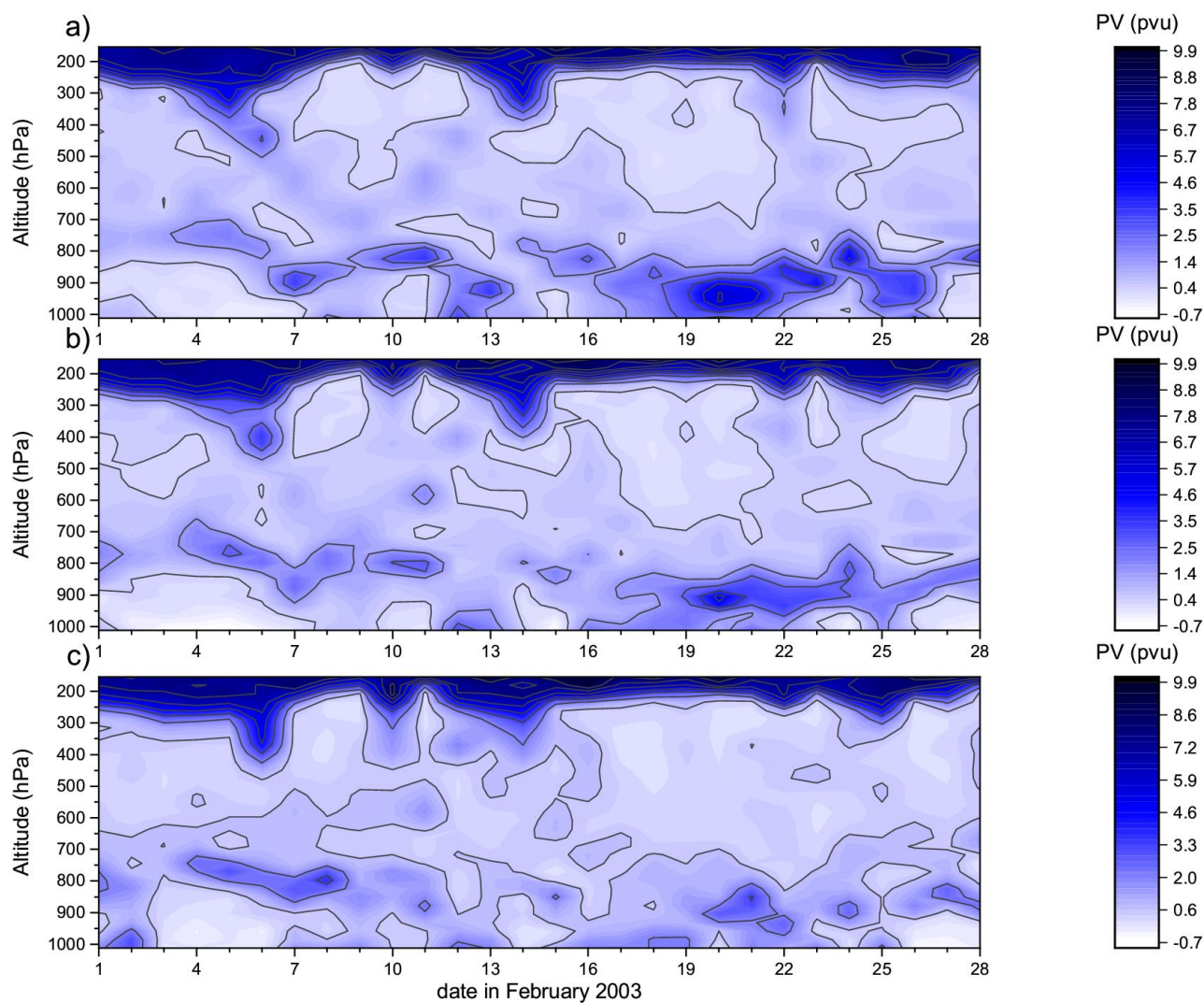
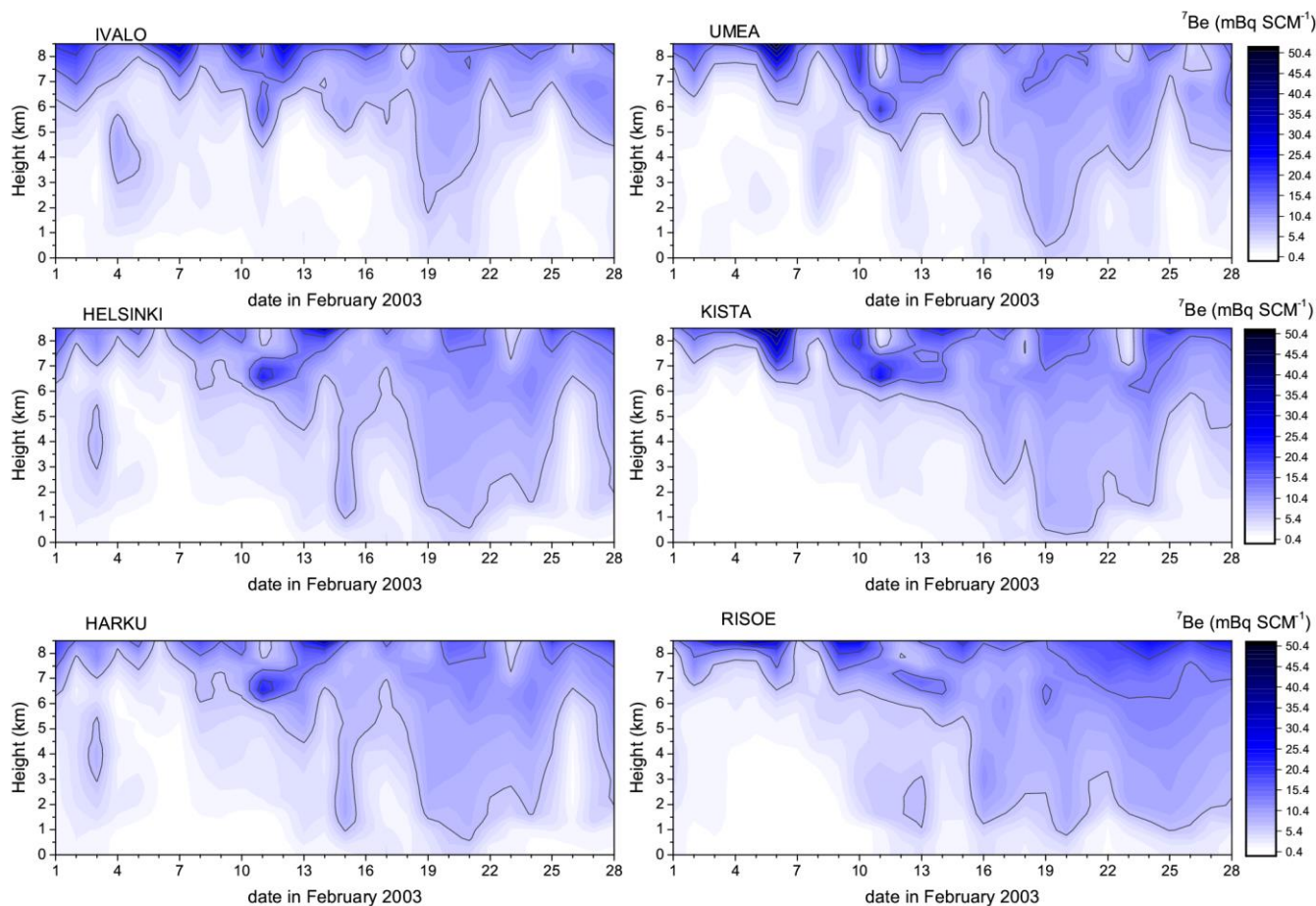


**Figure 9.** MERRA-2 daily mean relative humidity (colors) and winds (arrows) at ground level during February 18-25, 2003. The dots indicate the locations of the sampling sites: 1=Ivalo, 2=Umea, 3=Helsinki, 4=Kista, 5=Harku, 6=Risoe.



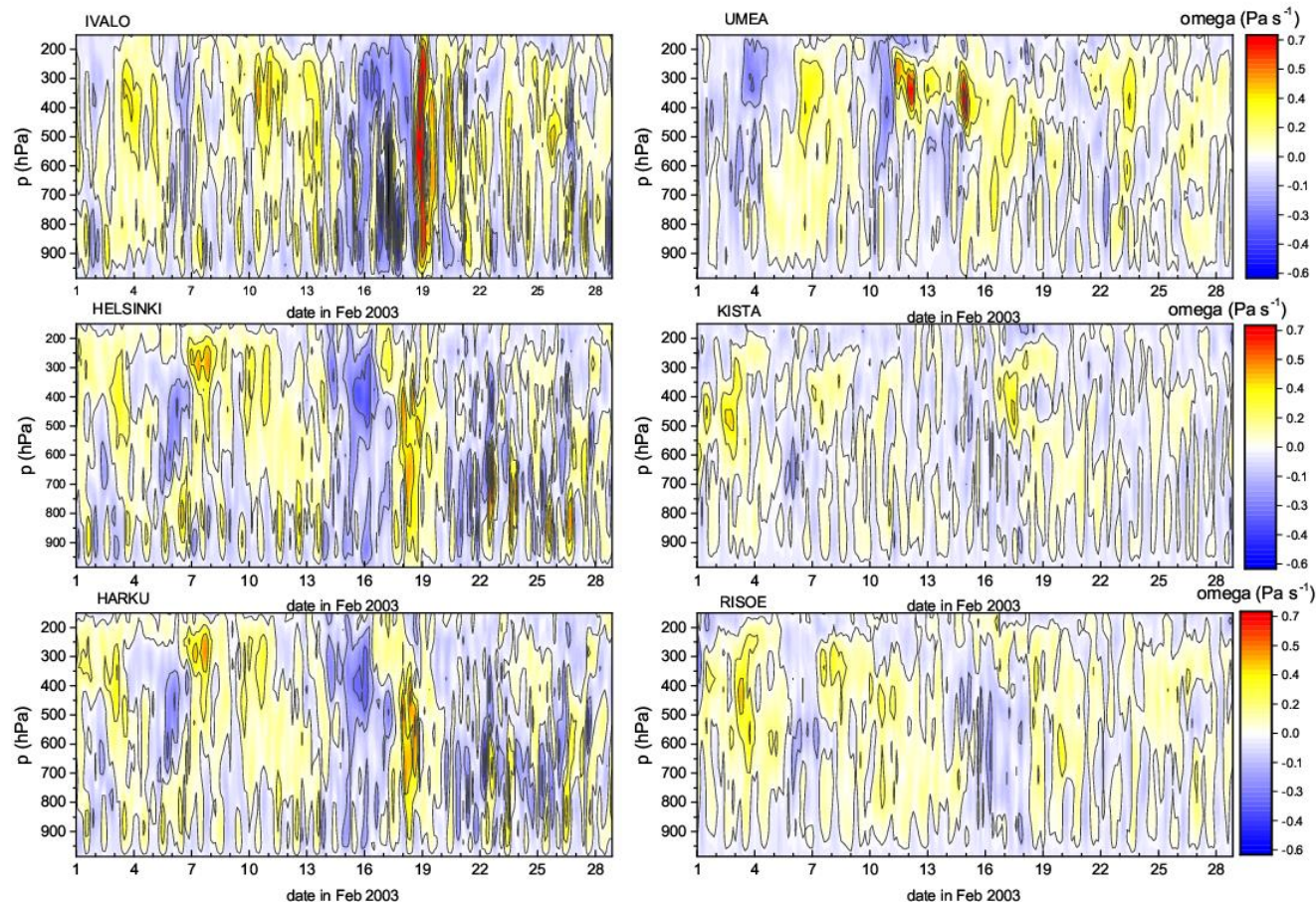
795

**Figure 10.** Time-height cross-sections of calculated daily potential vorticity during the month of February 2003 at three latitudes: a) 63°N, b) 64.5°N, and c) 66°N along the 21°E meridian.

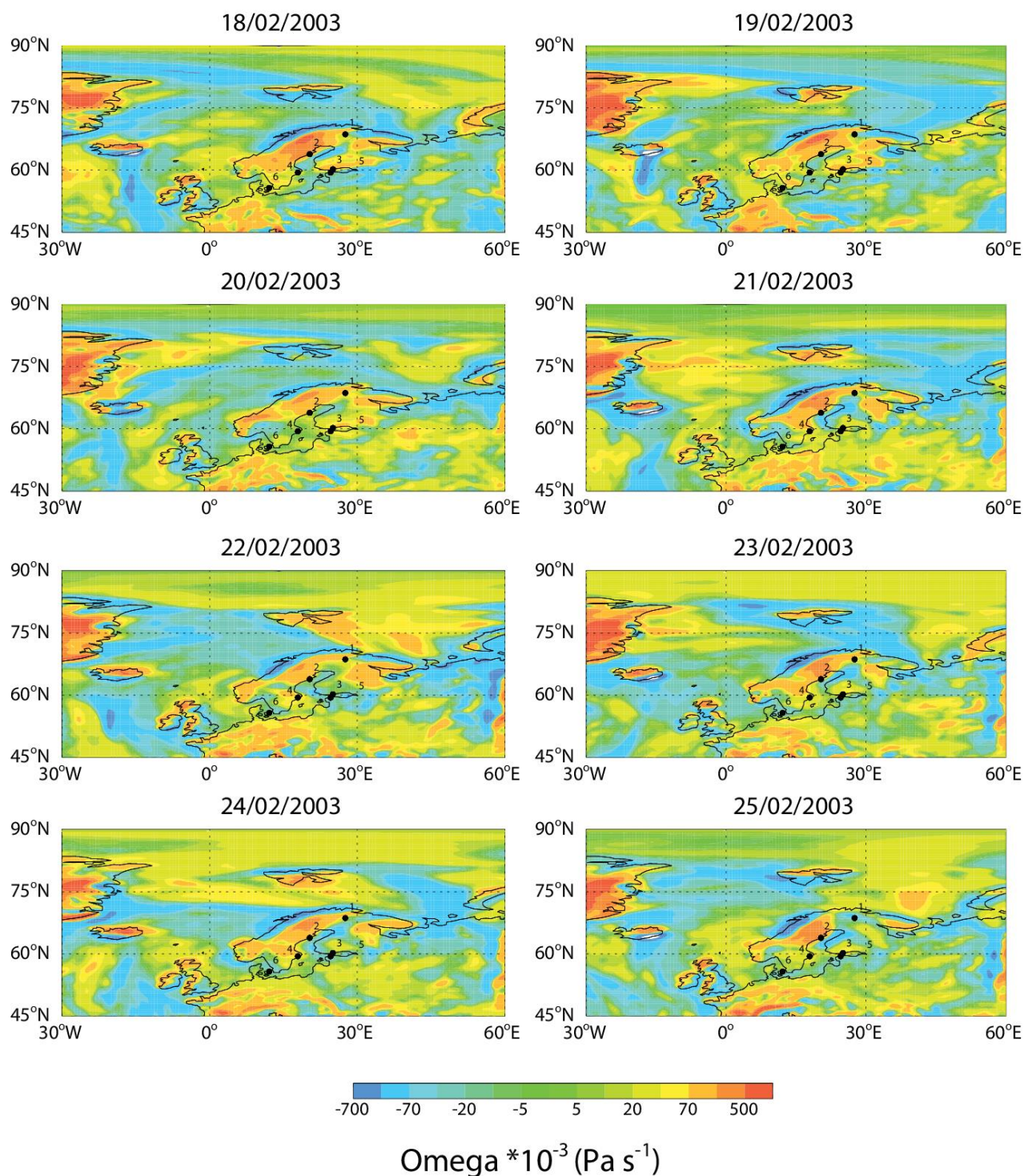


800 **Figure 11.** Time-height cross-sections of simulated hourly  $^7\text{Be}$  concentrations ( $\text{mBq SCM}^{-1}$  where SCM stands for Standard Cubic Meter) during the month of February 2003 at the six sampling sites.



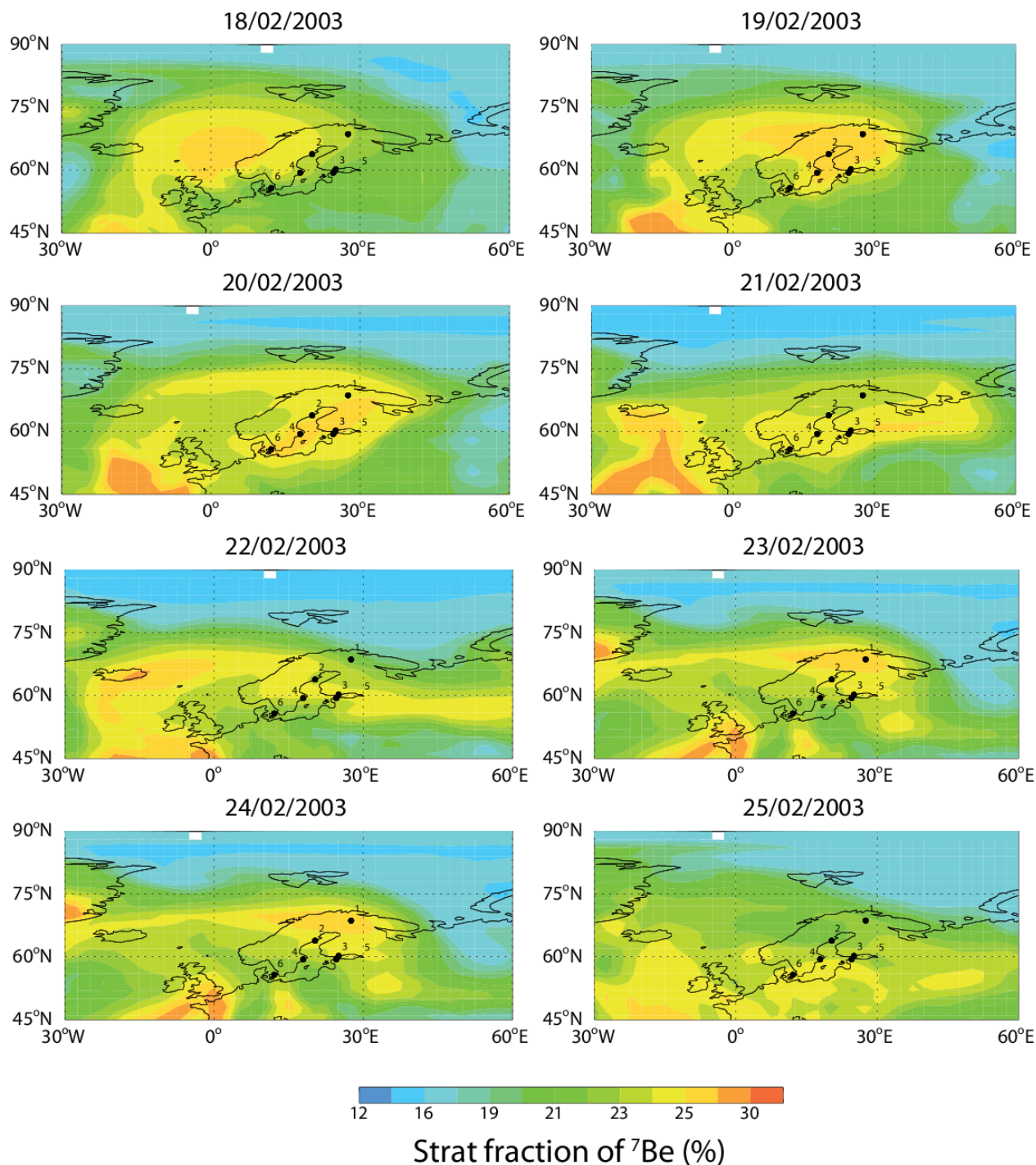


805 **Figure 12.** Time-height cross-sections of MERRA-2 3-hourly average pressure vertical velocity ( $\omega$ , in  $\text{Pa s}^{-1}$ ) during the month of February 2003 sampled at the six sampling sites.



810 **Figure 13.** MERRA-2 daily mean pressure vertical velocity ( $\omega$ ) at 940 hPa during February 18-25, 2003. The dots indicate the locations of the sampling sites: 1=Ivalo, 2=Umea, 3=Helsinki, 4=Kista, 5=Harku, 6=Risoe.





815 **Figure 14.** Simulated daily mean fraction of  $^7\text{Be}$  originating in the stratosphere (%) at 940 hPa. The dots indicate the locations of the sampling sites: 1=Ivalo, 2=Umea, 3=Helsinki, 4=Kista, 5=Harku, 6=Risoe.

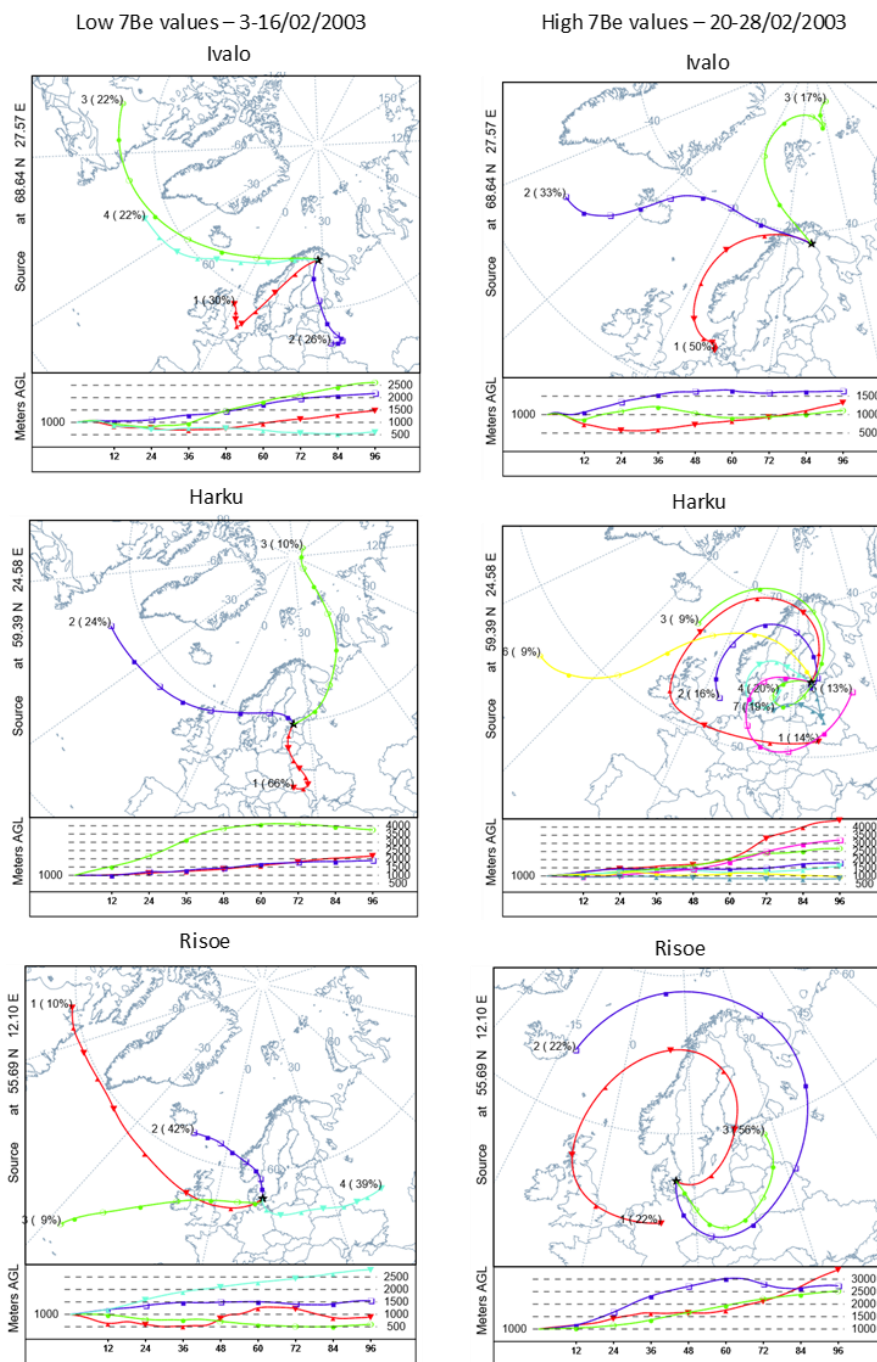


**Figure 15.** Average trajectory cluster results (centroids) in Ivalo, Harku and Risoe at 1000 m for low  $^7\text{Be}$  values (left: 3-16 February 2003) and high  $^7\text{Be}$  values (right: 20-28 February 2003), respectively. The stations are ordered by latitude from top to bottom (coordinates of the receptor site are provided on the left of each plot). The right numbers in the centroids are the percentage of complete trajectories occurring in that cluster, and the left numbers are an identification number of the centroid.